

VIBRATIONAL FREQUENCIES OF  
MAGNETIC RANDOM ACCESS MEMORY MATERIALS

LEE LI LING

DISSERTATION SUBMITTED IN FULFILMENT  
OF THE REQUIREMENTS  
FOR THE DEGREE OF MASTERS OF SCIENCE

DEPARTMENT OF PHYSICS  
FACULTY OF SCIENCE  
UNIVERSITY OF MALAYA  
KUALA LUMPUR

MAY 2010

# Abstract

The advantages of MRAM are so overwhelming which acts as motivation for scientist in further investigation for better read and write operation. The types of materials used are closely related to the cell performance in forming the ferromagnetic layers. Thus, the vibrational frequencies of the MRAM materials are of interest. Clusters for the two types of combinations,  $\text{Fe}_x\text{Ni}_y$  and  $\text{Fe}_x\text{Co}_y\text{B}_z$  are built. Subsequently, vibrational frequencies of each cluster are calculated theoretically from the first principles. The secular determinant is large when the number of electrons in a cluster is large. For the simplest combination of Fe-Ni cluster, (atomic number of an iron atom is 26 and a nickel atom is 28) gives secular determinant of  $26 \times 26$  and  $28 \times 28$  respectively. As the atomic number increases, the matrix becomes larger which is unlikely to be solved manually. These types of matrices are solved by a quadro computer operating at 2.83GHz with a good computer programme with suitable approximations. The density functional theory (DFT) is used to optimize the bond lengths and angles of the clusters for the minimum energy of the Schrödinger equation by using double zeta (DZ) and double zeta with polarized (DZP) wave functions. The bond distance calculated for cluster Fe-Ni is 213.4 picometer and the vibrational frequency shows a peak at  $316.5 \text{ cm}^{-1}$  (intensity = 0.002 km/mole). Larger size clusters show more vibrational frequencies. Cluster  $\text{Fe}_4\text{Co}_3\text{B}_4$  shows 16 peaks with the largest peak at  $1147.7 \text{ cm}^{-1}$ . The structure of the atomic combination is important in predicting which material works the best for memory performance. Calculations for several different ratios of the constituent atoms are performed.

# Abstrak

Kelebihan MRAM adalah sangat banyak di mana kelebihan tersebut merangsangkan ahli sains menjalankan penyelidikan dengan lebih terperinci untuk operasi baca dan tulis dengan lebih baik. Jenis bahan yang digunakan berkait secara rapat dengan prestasi sel dalam pembentukan lapisan feromagnet. Maka, frekuensi getaran bahan MRAMlah yang menarik minat. Dua jenis kombinasi kluster iaitu  $\text{Fe}_x\text{Ni}_y$  dan  $\text{Fe}_x\text{Co}_y\text{B}_z$  telah dibina. Seterusnya, frekuensi getaran bagi setiap kluster dikira berdasarkan teori dari prinsip pertama. Determinan sekular adalah besar apabila bilangan elektron dalam kluster besar. Kombinasi kluster Fe-Ni paling mudah, (nombor atom bagi atom ferum ialah 26 dan atom nikel ialah 28) memberikan determinan sekular masing-masing bernilai  $26 \times 26$  dan  $28 \times 28$ . Apabila nombor atom bertambah, matriks menjadi besar dan tidak boleh diselesaikan dengan manual. Sebaliknya, matriks jenis ini diselesaikan dengan komputer berkelajuan 2.83GHz bersamaan program yang baik dengan penganggaran yang sesuai. Teori fungsi ketumpatan mengoptimumkan panjang ikatan dan sudut kluster pada tenaga minimum bagi persamaan Schrödinger dengan menggunakan fungsi-fungsi gelombang zeta lipat dua dan zeta lipat dua dengan pengkutuban. Panjang ikatan bagi kluster Fe-Ni yang dikira oleh program ialah 213.4 pm dan puncak terunggul ditunjukkan pada frekuensi getaran  $316.5 \text{ cm}^{-1}$  (keamatan = 0.002 km/mole). Lebih banyak frekuensi getaran didapati bagi saiz kluster yang lebih besar. Kluster  $\text{Fe}_4\text{Co}_3\text{B}_4$  menunjukkan 16 puncak di mana puncak terbesar ialah  $1147.7 \text{ cm}^{-1}$ . Struktur dan kombinasi atom adalah penting dalam meramalkan bahan yang terbaik untuk kegunaan prestasi ingatan. Pengiraan bagi beberapa nisbah jujuk atom berlainan telah dijalankan.

# Acknowledgments

I would like to take this golden opportunity to express my sincere thanks to both my supervisors, Professor Dr. Keshav N. Shrivastava for sharing his knowledge and expertise and Professor Dr. Christopher G. Jesudason for useful discussions and for financial support.

I express my gratefulness to Dr. J. S. Van Gisbergen of the University of Amsterdam for providing the ADF computer programme. I also express my gratitude to the SCM group for discussions on the Amsterdam density functional (ADF) computer programme and problem solving.

I further wish to acknowledge my both seniors, Ahmad Nazrul Rosli and Noriza Ahmad Zabidi for giving me some ideas and knowledge about the ADF programme and the theories. Finally, I would like to thank my parents for constant support on my studies.

# Contents

<b>Abstract</b>	<b>ii</b>
<b>Abstrak</b>	<b>iii</b>
<b>Acknowledgements</b>	<b>iv</b>
<b>CHAPTER 1 Introduction</b>	<b>1</b>
1.1 Objective of research .....	1
1.2 Amsterdam Density Functional (ADF) .....	2
1.3 Overview .....	3
<b>CHAPTER 2 Magnetoresistive Random Access Memory (MRAM)</b>	<b>5</b>
2.1 Random Access Memory .....	5
2.2 Early MRAM devices .....	6
2.3 MRAM Description .....	7
2.3.1 GMR and TMR cells .....	8
2.3.2 MRAM using GMR cells .....	9
2.3.3 MRAM using TMR cells .....	10
<b>CHAPTER 3 Theory of molecules</b>	<b>12</b>
3.1 Density Functional Theory (DFT) .....	12
3.1.1 Overview of DFT .....	12
3.2 Geometry Optimization .....	16
3.3 Molecular Vibrations .....	17
3.3.1 Normal modes of vibration .....	18
3.3.2 The Classical Harmonic Oscillator .....	21
3.3.3 The Quantum Mechanical Harmonic Oscillator .....	22
<b>CHAPTER 4 Computerized Simulation of MRAM Material (<math>\text{Fe}_x\text{Ni}_y</math>)</b>	<b>24</b>
4.1 Introduction .....	24
4.2 Methodology .....	25
4.3 Clusters of $\text{Ni}_x\text{Fe}_y$ Atoms .....	25
4.4 Conclusions .....	31

<b>CHAPTER 5 DFT Calculation of Vibrational Frequencies of FeCoB</b>	<b>32</b>
<b>MRAM</b>	<b>32</b>
5.1 Introduction .....	32
5.2 Methodology.....	33
5.3 Clusters of Atoms .....	34
5.4 Conclusions .....	39
<b>CHAPTER 6 Large Clusters</b>	<b>40</b>
6.1 Introduction .....	40
6.2 Computational Results.....	40
6.2.1 Model 1.....	40
6.2.2 Model 2.....	43
6.2.3 Model 3.....	45
6.2.4 Model 4.....	48
6.2.5 Model 5.....	50
6.2.6 Model 6.....	52
6.2.7 Model 7.....	53
6.3 Analysis .....	54
6.4 Conclusions .....	55
<b>CHAPTER 7 Conclusions</b>	<b>56</b>
<b>List of Publications</b>	<b>60</b>
<b>Appendix A</b>	<b>61</b>
<b>Appendix B</b>	<b>62</b>
<b>Bibliography</b>	<b>81</b>

# List of Figures

2.3.1	The MRAM cell.....	7
4.3.1	The vibrational spectrum of NiFe <sub>3</sub> (pyramidal) calculated with polarized orbitals.....	26
4.3.2	Vibrational spectrum of Ni <sub>2</sub> Fe <sub>3</sub> (bipyramidal) calculated from the first principles.....	28
4.3.3	The vibrational spectrum calculated from the first principles using polarized orbitals of Ni <sub>4</sub> Fe <sub>3</sub> (boat shape).....	30
5.3.1	Vibrational spectrum of CoFeB <sub>2</sub> (triangular) calculated from the first principles.....	35
5.3.2	Spectrum of FeCoB <sub>2</sub> (triangular) calculated using DZP wave functions.....	36
5.3.3	Vibrational spectrum of FeCo <sub>2</sub> B (triangular).....	36
5.3.4	The vibrational spectrum of BFeCo <sub>2</sub> (triangular) calculated with polarized orbitals.....	37
5.3.5	The vibrational spectrum of CoBFe <sub>2</sub> (triangular) calculated from the first principles by using polarized orbitals.....	37
5.3.6	Vibrational spectrum of B-Co-B-Fe (rectangular) calculated by using DZP wave functions.....	38
5.3.7	Vibrational spectrum of FeCo <sub>2</sub> B (rectangular).....	38
5.3.8	Vibrational spectrum of Fe <sub>2</sub> CoB (distorted rectangular) calculated using DZP wave functions.....	39
6.2.1.1	The first spectrum on top and the second spectrum shows peaks of FeCoB <sub>3</sub> and Fe <sub>3</sub> CoB respectively calculated using double zeta polarized orbitals.....	41
6.2.2.1	Picture of cluster Fe <sub>2</sub> Co <sub>2</sub> B <sub>2</sub> .....	45
6.2.4.1	Picture and the vibrational spectrum of cluster FeCo <sub>3</sub> B <sub>4</sub> .....	48
6.2.6.1	Structure of cluster Fe <sub>3</sub> Co <sub>3</sub> B <sub>4</sub> and cluster Fe <sub>4</sub> Co <sub>3</sub> B <sub>3</sub> .....	52

# List of Tables

6.2.1.1	Frequencies and intensities of cluster $\text{FeCoB}_3$ and $\text{Fe}_3\text{CoB}$ calculated using DZ wave functions .....	41
6.2.1.2	Structures and bond lengths of clusters $\text{FeCo}_2\text{B}_2$ , $\text{Fe}_2\text{CoB}_2$ and $\text{Fe}_2\text{Co}_2\text{B}$ .....	42
6.2.2.1	Pictures and bond lengths of clusters $\text{FeCo}_2\text{B}_3$ and $\text{CoFe}_2\text{B}_3$ calculated using DFT simulations .....	44
6.2.3.1	Comparisons between cluster $\text{FeCo}_3\text{B}_3$ , $\text{Fe}_3\text{CoB}_3$ and $\text{Fe}_3\text{Co}_3\text{B}$ .....	47
6.2.3.2	Comparisons between cluster $\text{Fe}_2\text{Co}_2\text{B}_3$ and $\text{Fe}_3\text{Co}_2\text{B}_2$ .....	48
6.2.4.1	Bond lengths for cluster $\text{Fe}_3\text{CoB}_4$ , $\text{Fe}_3\text{Co}_3\text{B}_2$ , $\text{Fe}_3\text{Co}_4\text{B}$ and $\text{Fe}_4\text{Co}_3\text{B}$ ....	50
6.2.5.1	Cluster $\text{FeCo}_4\text{B}_4$ and $\text{Fe}_4\text{CoB}_4$ with their respective bond lengths .....	51
6.2.7.1	Comparisons between cluster $\text{Fe}_4\text{Co}_3\text{B}_4$ and $\text{Fe}_4\text{Co}_4\text{B}_3$ .....	54
4.3	The vibrational spectrum for clusters $\text{Ni}_x\text{Fe}_y$ from chapter 4 .....	62
5.3	Spectrum of small clusters $\text{Fe}_x\text{Co}_y\text{B}_z$ using double zeta spin polarized orbitals in chapter 5 .....	67
6.2.1	Spectrum for large clusters $\text{Fe}_x\text{Co}_y\text{B}_z$ in model 1 of chapter 6 .....	70
6.2.2	Spectrum for large clusters $\text{Fe}_x\text{Co}_y\text{B}_z$ in model 2 of chapter 6 .....	72
6.2.3	Spectrum for large clusters $\text{Fe}_x\text{Co}_y\text{B}_z$ in model 3 of chapter 6 .....	74
6.2.4	Spectrum for large clusters $\text{Fe}_x\text{Co}_y\text{B}_z$ in model 4 of chapter 6 .....	77
6.2.5	Spectrum for large clusters $\text{Fe}_x\text{Co}_y\text{B}_z$ in model 5 of chapter 6 .....	78
6.2.6	Spectrum for large clusters $\text{Fe}_x\text{Co}_y\text{B}_z$ in model 6 of chapter 6 .....	79
6.2.7	Spectrum for large clusters $\text{Fe}_x\text{Co}_y\text{B}_z$ in model 7 of chapter 6 .....	80



# CHAPTER 1

## Introduction

The discovery of the giant magnetoresistive (GMR) effect has given hope to the scientific community to build a memory device. The addition of GMR to the already existing memory technologies will be an advantage for the improved speed of the memory material. The magnetoresistive random access memory (MRAM) is believed to become a true universal non-volatile computer memory. Wonderful products are invented through the applications of MRAM in integrated circuits such as high storage devices on computers and notebooks, I-pods, mobile phones, military systems etc.

### 1.1 Objective of Research

MRAM performance is dependent on the magnetoresistance ratio (MR), where higher MR will have higher sensing signal and produce faster operation in the cell. Electron scattering in the ferromagnetic layers is believed to be an important factor affecting MR. When electric current passes through the ferromagnetic layers, the spins of the electrons get quantized in two possible ways; either spin-up or spin-down. Majority spin-up electrons pass through the cell with less scattering while the minority spin-down are strongly scattered. Thus, the less scattered electrons have lower resistance and the strongly scattered electrons have higher resistance. By determining the vibrational frequencies through simulation of clusters, force constant of the clusters can be achieved. The ability of electrons to be spin polarized on the ferromagnetic surface can

be observed. Therefore, the best materials for the ferromagnetic layers in the cell can be predicted on the basis of calculations of vibrational spectra.

An orbiting electron in an atom is like a circulating current and so has an associated orbital magnetic dipole moment. But not all the orbits produced the same magnetic moment. Different orbits have different effective currents and different effective areas. Iron possesses a net magnetic moment at the ground state. When the number of iron atoms in a cluster increases, the magnetization increases. However, when nickel (Ni) is added to the iron cluster, the magnetic moment or magnetization is affected. The total resistance is the measure of the cell's function, changes with the relative orientation of the two magnetic layers. It is thus of great importance to determine the materials used for the two ferromagnetic plates. In this research, faster read time access may be improved compared to the semiconductor device used nowadays.

In this research, the concentration of Ni is varied in Fe-Ni alloy and the material composition is found for which there is an extremum in the desired properties such as their vibrational frequencies, bond lengths and so on. The models of FeNi, FeNi<sub>2</sub>, FeNi<sub>3</sub>... Fe<sub>10</sub>Ni<sub>10</sub>, Fe<sub>9</sub>Ni<sub>11</sub>, Fe<sub>8</sub>Ni<sub>10</sub>, etc are made. Similar simulations are performed for Fe-Co-B also. The atoms of Fe, Co as well as B are varied to obtain Fe<sub>x</sub>Co<sub>y</sub>B<sub>z</sub> clusters. The vibrational frequencies of these clusters are then compiled and investigated.

## 1.2 Amsterdam Density Functional (ADF)

The ADF programme is used. It is based on the density functional theory (DFT) for ab initio calculations. Nowadays, ADF is often used in condensed-matter physics, computational physics and chemistry to determine the properties of materials which have applications in the industrial and in academic research.

The ADF programme can be applied to any gas phase molecules and molecules in protein environment. It can access all elements in the periodic table and can contain spin-orbiting methods etc. It is especially appropriate for transition metal and heavy nuclei compounds. A periodic structure complement to ADF is known as BAND is available to study chain, slab or bulk crystals and surfaces. At the same time, ADF programme is available to study frequency, density of states, potential energy surfaces and wide range of molecular properties. The programme solves the Schrödinger equation for any number of atoms in the density functional approximations. Usually, two approximations are available, the local density approximation (LDA) and the generalized gradient approximation (GGA). The GGA provides more excellent results for non-uniform models as gradients of the density at the same coordinate are also included. LDA depends only on the density at the coordinate. In this research, the clusters are assumed to be uniform. Hence, LDA calculations are used. There is a choice of several types of wave functions with and without spin polarization.

### 1.3 Overview

Chapter 2 is basically about MRAM history and the explanation on MRAM. RAM exists before MRAM. Due to the improvement in RAM technologies, MRAM is born and become dominant in the memory technologies.

Theory of molecules is described in chapter 3. A brief picture on how molecules behave in ground state and as well as in excited states and the approximations for the motion in molecular vibrations are mentioned. The theory used by the ADF programme also been described in brief with some equations and definitions.

Chapter 4 gives some of the results of the simulation of cluster  $\text{Fe}_x\text{Ni}_y$  where  $x=1, 2, 3$  and  $4$ . Spectra of these clusters and also the values of the vibrational frequencies with their intensities are shown.

Chapter 5 describes the clusters of  $\text{Fe}_x\text{Co}_y\text{B}_z$ . This chapter consists of clusters with 3 and 4 atoms. The figure of the clusters, bond lengths, vibrational frequencies and intensities are shown. Chapter 6 is the continuous part of chapter 5 but consists of clusters with total number of 5, 6, 7, 8, 9, 10 and 11 atoms which are categorized as large clusters. Lastly, chapter 7 gives the conclusions of the present study.

# CHAPTER 2

## Magnetic random access memory

### 2.1 Random access memory

Random access memory (RAM) can be quickly reached by the computer's processor which keeps the operating systems, application programs and data in current form. RAM is faster to read and write compared to other computer storages. Whereas, one of the weaknesses of RAM is often related to volatile types of memory where the data contained is lost when the computer is switched off. RAM is known as random access as it takes the form of integrated circuit which allows data to be read from or written to in any order despite the physical location and the relation to the previous data.

RAM can be described as human's short-term memory while hard disk as the long-term memory. RAM never runs out of memory. When the RAM is filled up, the computer's operation becomes slow as the processor needs to refresh data from the hard disk. For the long-term memory, there is limitation for data storage capacity.

Although RAM usually related with those volatile types of memory such as dynamic random access memory (DRAM) and static random access memory (SRAM), they are also available for non-volatile types of memory. For example, the non-volatile types of memory are the read only memory (ROM), Flash memory and most types of magnetic storage (hard disks, floppy disk and etc.)

## 2.2 Early MRAM devices

The natural hysteresis as a function of the magnetic field is used for data storage by using two or more sets of current-carrying wires. This describes the basics of magnetic random access memory (MRAM). Most of the latest MRAM are still using the same concept. The magnetic layers were arrayed so that those cells to be written received a combination of magnetic field while the other layers in the array do not change the storage data. Early ferrite core use binary digits for data storage (“1” or “0”). A magnetic field was used to interrogate the memory element and the polarity of the induced magnetic element will determine whether a “1” or “0” was stored.

Raffel and Crowder [1] were the first to propose a magnetoresistive readout scheme. The scheme stored data in magnetic body, in turn produced stray of magnetic field which could be detected by a separate magnetoresistive sensing element. But this does not work out as it is difficult to obtain a sufficiently large external stray field from small magnetic storage cell. Cross-tie Cell Random Access Memory (CRAM) [2] was then introduced which used magnetic element for storage and magnetoresistive readout. But yet there are difficulties in getting the cell to write consistently and the difference between “1” and “0” is small. In mid 1980’s, Honeywell developed the first MRAM device based on magnetoresistance using Anisotropic Magnetoresistance (AMR) materials. The angle of the electrical current with respect to the orientation of magnetic field which alters the electrical resistance of the cell is the property of an AMR material. With recent advance in MRAM nowadays, better materials were developed such as Giant Magnetoresistance (GMR) and Tunnel Magnetoresistance (TMR) materials. These materials are significant in our existing technology where these materials are applied in our electrical appliances we are using every day.

## 2.3 MRAM Description

Magnetoresistive random access memory (MRAM) has been developed since 1990s. MRAM technology combines the ability of performance, low power and non-volatility. MRAM has theoretically an unlimited read and write capability. Akerman [3] mentioned that the advantages of MRAM become dominant for all types of memory, thereby becoming a truly “universal memory”.

RAM data is stored as an electric charge or current flow. But for MRAM, data is stored by magnetic storage elements. Data storage is determined by the state of the binary digits, either “1” or “0”, which is the basic information unit in a computer. The bits are recorded using the magnetic storage elements comprising one or more ferromagnetic layers associated to the cell. One of the layers is programmable (free magnetic layer) where the layer can change the magnetic field between two possible orientations. The magnetization of other or more layers remain unchange which is known as pinned magnetic layer. The two layers is separated by a nonmagnetic spacer layer. Figure 2.3.1 shows a brief picture of the MRAM cell.

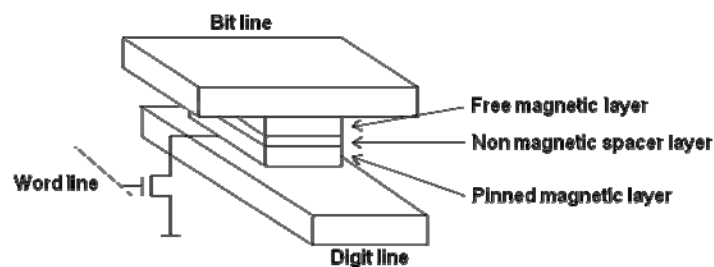


Figure 2.3.1. The MRAM cell.

As other semiconductor memory types, the MRAM core is one or more of 2-D array of storage cells. Multiple arrays shorten the signal paths and thus speed up the access time [4]. The rows in each array are traversed by the parallel word lines in one direction while the columns are traversed by the bit lines running in the orthogonal

direction to the word lines. Cross points of the word lines and bit lines are the magnetic memory cell where the cell can be identified or accessed easily.

Chip performances are determined by write and read operations. Write operations can be achieved by the induced magnetic field created by the free layer when the current is driven along the bit lines, word lines or digit lines. Read operations are achieved by measuring the electrical resistance of the cell. If the applied magnetic field causes the angle between the pinned layer and the free layer to change, the resistance varies, showing the magnetoresistance (MR) effect. The MR ratio is important in determining the MRAM's quality. The MRAM development effort has been required up to over MR ratio of 40% compared to a few percent for the previous years. Magnetoresistance ratio,  $MR = \frac{(R_{\max} - R_{\min})}{R_{\min}} \times 100\%$ , where  $R_{\max}$  and  $R_{\min}$  is the maximum and minimum value of the magnetoresistance of the cell respectively.

### 2.3.1 GMR and TMR cells

The breakthrough of GMR effect in metal multilayer encourages researches and scientists in the development of computer memory technologies. Successful GMR in MRAM devices act as a motivation for researches to study the MR effects in TMR. Experiments done show that the MR ratio of TMR device was much higher compared to GMR device with the value larger than 20%.

GMR and TMR cell holds a common structure which is constructed by two ferromagnetic metal layers that are separated magnetically by a nonmagnetic layer. The difference between the two cells is that the nonmagnetic layer of a GMR cell consists of a metal layer while that of TMR cell consists of an insulator layer. The effect of the common structure can be observed through the change in the electrical resistance. Magnetization varies when the ferromagnetic layers vary with different angles, from



low to high or high to low resistance. There are two different methods to alternate the resistance across the cell:

(i) Spin-pinning method:

An antiferromagnet layer is placed on the surface of the ferromagnetic layer to pin its orientation, while the other layer is free to rotate with the applied field. The device used in this method is known as spin valve. TMR is much likely the extension of the spin valve GMR.

(ii) Using ferromagnetic layers with different coercive force:

Both the ferromagnetic layers will orientate to a parallel and antiparallel state at a small field if the coercive force is different from each another. The type of device is known as pseudo spin valve (PSV).

These two methods have used GMR in the MRAM devices due to their simple structure and low working fields.

### 2.3.2 MRAM using GMR cells

Discovery of GMR effect has arise hope for the scientific community. While we were still wondering the mysterious technology on how electrical resistance changes when an applied field acts on ferromagnetic materials, Albert Fert and Peter Grunberg independently discovered the GMR effect [5, 6]. Through intense work by the scientist and researchers, magnificent products are invented such as high storage device on computers and notebooks, I-pods, mobile phones, etc.

The physics of GMR was the spin-dependent scattering of the electrons in the ferromagnetic layers [7]. The GMR cells yet show limitations. The read access time was much slower compared to the semiconductor memory due to the low signal. Invention of pseudo spin valve (PSV) cell improves the GMR cell. PSV cells consist of two magnetic layers with different coercivity insulated by a nonmagnetic metal layer [8,

9]. Coercivity measures the resistance of a ferromagnetic material to becoming demagnetized. Different coercive force can be defined as different thickness of magnetic layers where thinner layer is known as the soft ferromagnetic layer and thicker layer as the hard ferromagnetic layer. Usually soft ferromagnetic materials have low coercivity and switch at lower field while hard materials have high coercivity and switch at higher field. For PSV cell which is at low field, the layer with low coercivity is more susceptible to the magnetization change than the layer with high coercivity. Thus, the data are stored in the hard ferromagnetic layer and the resistance of the cell can be modified by the soft ferromagnetic layer.

### 2.3.3 MRAM using TMR cells

Magnetic Tunnel Junction (MTJ) cell or the spin valve MRAM cell holds common structure as GMR cell. This component consists of four layers. The orientation of the magnetic field of one of the ferromagnetic layer is pinned by the existence of the fourth antiferromagnetic layer formed on the surface of that ferromagnetic layer. The other layer so called the free layer will modify its magnetic field to match that of the layer with fixed magnetic polarity. The free layer is also known as the rotating layer due to the circulation of the magnetic field. Both the pinned and free layers are separated by an insulating metal often made from copper.

The theoretical basic of MTJ cell was the tunnel magnetoresistance [10-13] which produces a magnetoresistive effect. As a result of the wave-like nature of electrons, the spins travel perpendicularly to the layers across the thin insulating tunnel barrier. The tunneling conductance depends on the density of states (DOS) of the spins at Fermi level of the ferromagnet layers. Due to the tunneling effect, MTJ cell attained larger impedance and therefore lower current flows across the cell and higher MR effect is produced. Thus, the TMR devices have advantages over GMR device for high

speed non-volatility MRAM memory. Nowadays, the TMR devices have replaced the GMR devices in disk drives.

# CHAPTER 3

## Theory of molecules

### 3.1 Density functional Theory (DFT)

Density functional theory (DFT) description for ground state properties of metals, semiconductors and insulators is now very popular. The main idea of DFT is to describe an interacting system of electrons via electron density. The wave function ( $\psi$ ) of an N-electron system includes  $3 \cdot N$  degrees of freedom, while the density, no matter how large the system is, contains only 3 spatial coordinates ( $x, y, z$ ). The computational effort is simplified moving from  $E(\psi)$  to  $E(\rho)$  in terms of the electronic properties of clusters. DFT also provides various chemical properties, such as electronegativity (chemical potential), hardness (softness), response function, etc. These important concepts can conveniently explain chemical properties upon change of nuclei.

The DFT in principle provides good ground state description. It is based on approximations used to calculate exchange-correlation potential which will be discussed below. The exchange-correlation energy describes the effect of Pauli principle and Coulomb potential beyond the pure electrostatic interaction of electrons.

#### 3.1.1 Overview of DFT

Density functional theory (DFT) can be regarded as the exactification of the two Hohenberg-Kohn theorems. Its basic concepts are developed from the Thomas-Fermi model which was introduced in 1927 [14, 15, 16, 17]. It is a quantum mechanical

theory for the electronic structure of many body systems, developed after the Schrödinger equation was introduced. The model was a statistical model using mathematical basis to approximate distributions of electrons in a solid. They assumed the existence of energy functional, and the kinetic energy based on the density of electrons,  $\rho(\vec{r})$  which was derived in an infinite potential well. The functional of kinetic energy based on electron density,  $T_{TF}(\rho)$ :

$$T_{TF}(\rho) = \frac{3}{10} (3\pi^2)^{2/3} \int d\vec{r} \rho^{5/3}(\vec{r}) \quad (1)$$

$$= C_F \int \rho^{5/3}(\vec{r}) d\vec{r} \quad , \text{ where } C_F = \frac{3}{10} (3\pi^2)^{2/3}$$

While the energy of an atom using kinetic energy functions with electron-nucleus attraction, electron-electron repulsion and Hartree energy can be calculated. Thus, the Thomas- Fermi energy,  $E_{TH}(\rho)$ :

$$E_{TH}(\rho) = T_{TF}(\rho) - Z \int d\vec{r} \frac{\rho(\vec{r})}{|\vec{R} - \vec{r}|} + \frac{1}{2} \iint d\vec{r}_1 d\vec{r}_2 \frac{\rho(\vec{r}_1)\rho(\vec{r}_2)}{|\vec{r}_1 - \vec{r}_2|} \quad (2)$$

$Z$ = nuclear charge,  $R$ = position vector of the nucleus,  $\vec{r}$  = position vector of an electron

Thomas-Fermi model is limited and only correct in an infinite nuclear charge. Edward Teller (1962) showed that Thomas-Fermi theory does not predict any molecular bonding. The energy calculated of any molecule with Thomas-Fermi theory is much higher than the sum of the energies of the constituent atoms. Since this precision is not good for atoms, the Hohenberg-Kohn theorem was proposed around 1965.

Hohenberg-Kohn theorem relates to that any system consisting of non-degenerate ground state of electron moving under an external potential  $V_{ext}(\vec{r})$  with the absence of magnetic field, where the external potential  $V_{ext}(\vec{r})$  is a unique function of  $\rho(\vec{r})$ .

Theorem 1: Through the use of the function of electron density  $\rho(\vec{r})$ , the ground state properties of a many-electron system are uniquely determined by the electron densities that depend on the three spatial coordinates. It lays the ground work for reducing the many-body problem of N electrons with 3N spatial coordinates.

Theorem 2: The ground state energy can be obtained variationally [18]: the density that minimizes the total energy is the exact ground state density.

Hohenberg-Kohn theorems are useful, but the existence of theorem is not enough as the way in computing the ground-state density of a system is not offered. Soon, Kohn and Sham (one particle DFT) [19] devised a simple method for carrying-out the DFT calculations. The comparison between DFT theory and the Hartee-Fock theory makes a clearer picture about the deviations of them as given below.

Initially, the DFT starts from the total energy function,  $E=E[\rho, R_\alpha]$ , where the electron density  $\rho(\vec{r})$  is a physically observable fundamental quantity [20]. In contrast, to the Hartee-Fock theory (HF) which starts from the total energy containing the wave function,  $E=E[\Psi, R_\alpha]$ .

$$E = \int \Psi^* \left[ \sum_i h_i + \sum_{i>j} 1/r_{ij} \right] \Psi d\tau \quad (\text{HF theory}) \quad (3)$$

$$E = T[\rho] + U[\rho] + E_{xc}[\rho] \quad (\text{DFT theory}) \quad (4)$$

The total energy for the HF theory is expressed as an expectation value of the exact non-relativistic Hamiltonian [21] using the Slater determinant [22] as approximation for the total  $\Psi$ . The total energy of DFT theory is decomposed into three terms, kinetic energy term  $T[\rho]$ , Coulomb energy term  $U[\rho]$  and the many-body exchange correlations term  $E_{XC}[\rho]$ .

For the HF theory, the total wave function is given as  $\psi = |\psi_1(1), \psi_2(2), \dots, \psi_n(n)\rangle$ , and the electron density derived as  $\rho(\mathbf{r}) = \sum_{\text{occ}} |\psi_i(\vec{r})|^2$  for the DFT theory.

$$\left[-1/2\nabla^2 + V_c(\vec{r}) + \mu_x^i(\vec{r})\right] \Psi_i = \varepsilon_i \Psi_i \quad (\text{HF equation}) \quad (5)$$

$$\left[-1/2\nabla^2 + V_c(\vec{r}) + \mu_{xc}(\vec{r})\right] \Psi_i = \varepsilon_i \Psi_i \quad (\text{Kohn-Sham equation}) \quad (6)$$

Both equations are quite similar. In HF theory, the difference is  $\mu(\vec{r})$  which describes the exchange effects and depends on the actual orbital. The Kohn-Sham equations:

- (i) charge density,  $\rho(\vec{r}) = \sum_i^N \sum_s |\Psi_i(\vec{r}, s)|^2$ ,
- (ii) Schrödinger equation for N non-interacting electron moving in an effective potential  $V_{\text{eff}}(\vec{r})$ ,  $\left[-1/2\nabla^2 + V_c(\vec{r}) + \mu_{xc}(\vec{r})\right] \Psi_i = \varepsilon_i \Psi_i$  and
- (iii) the effective potential,  $V_{\text{eff}}(\vec{r}) = V_{\text{ext}}(\vec{r}) + e^2 \int \frac{\rho(\vec{r}')}{|\vec{r} - \vec{r}'|} d\vec{r}' + \frac{\delta E_{xc}[\rho]}{\delta \rho}$

are sets of eigenvalues in the DFT. The energy functional  $E[\rho(\vec{r})]$  postulated by Kohn and Sham [19] could be written as:

$$E[\rho(\vec{r})] = T_c[\rho(\vec{r})] + \frac{e^2}{2} \iint \frac{\rho(\vec{r})\rho(\vec{r}')}{|\vec{r} - \vec{r}'|} d^3\vec{r} d^3\vec{r}' + E_{xc}[\rho(\vec{r})] + e \int \rho(\vec{r}) V_{\text{ion}}(\vec{r}) d^3(\vec{r}) \quad (7)$$

where,  $T_c[\rho(\vec{r})]$  = Kinetic energy of a system of non-interacting electrons with density  $\rho(\vec{r})$  and  $V_{\text{ion}}$  = potential energy due to static ions.

These equations are solved iteratively to obtain self-consistency.

Local density approximation (LDA) is the simplest approximation of Kohn-Sham theory which is based upon the exchange-correlation (XC) energy functional for a uniform gas at each space point via electron density. LDA is also used in the Amsterdam Density Functional (ADF) programme for calculating the first principle of electronic structures. LDA is derived successfully from the homogeneous electron gas (HEG) model. Thus, the LDA is identical to the HEG approximation which is applied to molecules and solids.

LDA exchange-correlation energy for spin-unpolarized system is defined as  $E_{xc}^{\text{LDA}}[\rho] = \int \rho(\vec{r}) \varepsilon_{xc}(\rho) d\vec{r}$ , where  $\rho$  is the electron density and  $\varepsilon_{xc}$  is the exchange-

correlation energy density. When the system is extended to spin-polarizing, further approximation is needed for correlation and exchange can be determined by the known spin-scaling. Two spin-densities  $\rho_\alpha$  and  $\rho_\beta$  can form the local-spin-density approximation which is defined as  $E_{XC}^{LSDA}[\rho_\alpha, \rho_\beta] = \int d\vec{r} \rho(\vec{r}) \epsilon_{XC}(\rho_\alpha, \rho_\beta)$  and  $\rho = \rho_\alpha + \rho_\beta$ . Adding spin-polarization, the spin dependence of the correlation energy density can be defined as:

$$\xi(\vec{r}) = \frac{\rho_\alpha(\vec{r}) - \rho_\beta(\vec{r})}{\rho_\alpha(\vec{r}) + \rho_\beta(\vec{r})} \quad (8)$$

$\xi = 0$ , paramagnetic spin-polarized situation with equal  $\alpha$  and  $\beta$  spin densities

$\xi = 1$ , ferromagnetic situation when one spin density vanishes

## 3.2 Geometry Optimization

The geometry of molecules determines its physical and chemical properties. Usually, the bond angles, bond lengths and dihedral angles are optimized. According to the VSEPR (valence shell electron-pair repulsion) model, the geometry of the molecule is determined by the repulsive forces of valence electron pairs which directly affect the size of the bond angle. The stronger the repulsion length, the larger is the bond angle. Arrangement of atoms in the molecules determines the energy levels of those molecules. In fact, even small changes in the structure cause the energy in a molecular system to vary. The objective of the geometry optimization is to find the point at which the energy is at a minimum where the molecule is the most stable and most likely to be found in nature.

The way to observe the effect of different geometries on energy levels is to calculate a potential energy surface (PES). The PES is a mathematical relation correlating the particular molecular structure and its point energy. The purpose of geometry optimization is to locate the minima based on the geometry of the molecule.



The forces are zero at the point on the potential energy surface when it reaches a stationary point. It is done by calculating the first derivative of the energy (gradient).

Usually user begins the geometries of a cluster as Cartesian coordinates. When a basis set is specified, the programme will compute the energy and the gradient at the point, decide whether it reached a stopping point (convergence) and the geometry varies based on the size of the gradient. The new integrals are calculated, new self-consistent field (SCF) calculations are done, and a new energy and gradient are calculated. These steps are repeated until the programme reaches convergence.

### 3.3 Molecular Vibrations

Molecular vibrations are delineated as motion of atoms in the molecule which are constantly moving with respect to each other in a periodic form while the molecule as a whole has a constant translational and rotational motion. The frequency of the periodic motion is known as the vibrational frequency. The molecular vibration is excited when the molecule at the ground state absorbs a quanta of energy,  $E = h\nu$ , where  $\nu$  = frequency and  $h$  = Planck's constant. When two quanta of energy are absorbed, the first overtone is excited and so on to higher overtones.

The first approximation for the motion in a normal vibration is the simple harmonic motion. The vibrational energy is a quadratic function with respect to the atomic displacement and the first overtone with frequency  $2\nu$ . But in reality, the vibrations are anharmonic and the first overtone has less energy than  $2\nu$  frequency.

The normal modes are a set of  $3N-6$  collective atomic displacements which is used to describe the overall vibrational motion of the molecule. The normal modes are independent of each other, each represent motions of different parts of the molecule.

### 3.3.1 Normal modes of vibration

Normal modes are usually the combination of motions involving all atoms to varying degrees which move sinusoidally with the same frequency known as natural frequency or resonant frequency. The harmonic system can be used to illustrate the frequency of the normal mode of a molecule. When a molecule is excited at a frequency,  $\nu$ , all of the atoms will also move at the same frequency. The phases movement are exactly in phase or in the opposite phase.

To obtain the frequencies and coordinates of the normal modes of a polyatomic molecule through basic theoretical derivations, the classical equation of motion for normal coordinates is initially derived. The normal coordinates can be expressed as linear combinations of the Cartesian atomic displacements. The classical expression for the total energy,  $E = \text{kinetic energy (K.E)} + \text{potential energy (V)}$  of a collection of  $N$  atoms is formed [23]. The kinetic energy is given as

$$T = \frac{1}{2} \sum_{i=1}^N m_i (\dot{x}_i^2 + \dot{y}_i^2 + \dot{z}_i^2) = T_{\text{trans}} + T_{\text{rot}} + T_{\text{vib}} \quad (9)$$

The kinetic energy above comprises the translational, rotational and vibrational degrees of freedom. The potential energy is

$$\begin{aligned} V = V_0 + \sum_{i=1}^N \left[ \left( \frac{\partial V}{\partial x_i} \right)_0 x_i + \left( \frac{\partial V}{\partial y_i} \right)_0 y_i + \left( \frac{\partial V}{\partial z_i} \right)_0 z_i \right] \\ + \frac{1}{2} \sum_i \left[ \left( \frac{\partial^2 V}{\partial x_i^2} \right)_0 x_i^2 + \left( \frac{\partial^2 V}{\partial y_i^2} \right)_0 y_i^2 + \left( \frac{\partial^2 V}{\partial z_i^2} \right)_0 z_i^2 \right] \\ + \frac{1}{2} \sum_{i,j=1}^N \left[ \left( \frac{\partial^2 V}{\partial x_i \partial y_j} \right)_0 x_i y_j + \left( \frac{\partial^2 V}{\partial y_i \partial z_j} \right)_0 y_i z_j + \left( \frac{\partial^2 V}{\partial z_i \partial x_j} \right)_0 z_i x_j \right] \end{aligned} \quad (10)$$

The  $V_0$  may be assumed to be zero and first derivatives vanish at equilibrium geometry.

The position of the center of mass is preserved when the normal coordinates are obtained so that the energies are expressed in mass-weighted Cartesian coordinates.

These are defined as:  $\eta_1 = \sqrt{m_1} x_1$ ,  $\eta_2 = \sqrt{m_1} y_1$ ,  $\eta_3 = \sqrt{m_1} z_1$ ,

$$\eta_4 = \sqrt{m_2} x_2, \dots, \eta_{3N} = \sqrt{m_N} z_N$$

The general relationship of force constant can be defined as:  $b_{ij} = \frac{\partial^2 V}{\partial x_i \partial y_j}$ .

If the coordinates of  $i$  and  $j$  are the same, the force constant is known as the principal force constant. While if the coordinates of  $i$  and  $j$  are different, the force constant is an interaction constant since it is related to the way in which the two coordinates interact with each other. Kinetic and the potential energies are expressed as:

$$T = \frac{1}{2} \sum_{i=1}^{3N} \dot{\eta}_i^2 \quad (11)$$

$$V = \frac{1}{2} \sum_{i,j}^{3N} b_{ij} \eta_i \eta_j, \quad b_{ij} = \text{elements of the force-constant matrix } \mathbf{B}. \quad (12)$$

There are  $3N$  classical equations of motion for the system.

$$F_{x,i} = \frac{d}{dt}(m\dot{x}_i) = \frac{-\partial V}{\partial x_i} \quad (13)$$

$F_{x,i}$  gives a force on atom  $i$  in the  $x$ -direction.

Substituting the mass-weighted Cartesian coordinates and the force constants  $b_{ij}$ , the equation of motion are as follows:

$$\frac{d}{dt} \dot{\eta}_i + \sum_j b_{ij} \eta_j = 0. \quad (14)$$

We expect that the motion is harmonic for a quadratic field, thus after integration, we obtain,

$$\eta_i = \eta_i^0 \sin(\sqrt{\lambda}t + \delta). \quad (15)$$

where  $\omega = 2\pi\nu \equiv \sqrt{\lambda}$ ,  $\eta_i^0$  = amplitude and  $\delta$  = phase of the oscillation. Both  $\eta_i^0$  and  $\delta$  are constants of integration which depend on the boundary.

The equation for  $i=1$  to  $3N$ , where  $-\lambda\eta_i^0 + \sum_j b_{ij}\eta_j^0 = 0$  is obtained when equation (2)

is substituted into equation (1). The equation can be written as a matrix equation where

$(\mathbf{B}-\lambda\mathbf{I})\eta^0 = 0$ . A nontrivial solution to the set of equations can be expressed in

$\det(\mathbf{B}-\lambda\mathbf{I})\eta^0 = 0$  if only the determinant of the matrix is zero. Solving the nontrivial solution is also the procedure of finding the normal coordinates and their frequencies. From  $(\mathbf{B}-\lambda\mathbf{I})\eta^0 = 0$ , we define  $\mathbf{I}$  as the identity matrix and  $\eta^0$  is a column vector containing the amplitudes of the mass-weighted Cartesian coordinates.

In the matrix notation, potential energy is expressed as  $V = \frac{1}{2}\eta^T \mathbf{B} \eta$ , where  $\eta^T$  is the transpose of  $\eta$ . After diagonalizing the potential energy or by means of transformation to normal coordinates,  $Q_i$ , stated each normal coordinate as a linear combination of the mass-weighted Cartesian coordinates [24].

$$Q_i = \sum_{k=1}^{3N} l_{ki} \eta_k, \text{ where } l_{ki} \text{ are the coefficient to be determined.}$$

The matrix equation of  $Q_i$  is expressed as  $\mathbf{Q} = \mathbf{L}^T \eta$ , given that  $\mathbf{Q}$  is a column vector containing normal coordinates and  $\mathbf{L}^T$  is the transpose of  $\mathbf{L}$ . The quantum mechanical operators can be substituted for the classical expression for the position and momentum. A  $3N-6$  independent and one dimensional equations are obtained, which forms familiar harmonic oscillator Schrödinger equation. Thus, a normal analysis provides a set of normal modes, their frequencies related to the masses of atoms, geometry of molecules and force constants of bonds. Usually these calculations are solved by the computers with good programme as they are unlikely to be solved manually.

In general, the force constant is used as an input for the calculation. The force constant is not available from the experimental process, but can be determined by fitting the calculated values to the observed vibrational frequencies. Besides that, force constant also can be determined through quantum mechanical calculation of the energy of an electronic state (ground state) as a function of the geometry.

### 3.3.2 The Classical Harmonic Oscillator

The molecular vibrations can be treated using the Newtonian mechanics to calculate frequencies,  $\nu$ . The basic assumption is that each vibration treated corresponds to a spring. The harmonic approximation obeys the Hooke's law. The force on the spring is directly proportional to the displacement (change in bond length).

$$F = -fq$$

The negative sign indicates that  $F$  is the restoring force which acts in a direction opposite to the displacement and  $f$  is the force constant. Thus, the force exerted by the spring will cause the atoms to return to their original position.

Equating Newton second law of motion to the exerted force,

$$F = ma = m \frac{d^2q}{dt^2} = -fq$$
$$m \frac{d^2q}{dt^2} + fq = 0.$$

We use the differential equation to solve it,

$$q = q_0 \cos(2\pi\nu t + \phi)$$

$$\dot{q} = -2\pi\nu q_0 \sin(2\pi\nu t + \phi)$$

$$\ddot{q} = -4\pi^2\nu^2 q_0 \cos(2\pi\nu t + \phi) = -4\pi^2\nu^2 q.$$

The  $\ddot{q}$  is substituted into  $m \frac{d^2q}{dt^2} + fq = 0$

$$m(-4\pi^2\nu^2 q) + fq = 0, q \neq 0$$

$$\therefore \nu = \frac{1}{2\pi} \sqrt{\frac{f}{m}}.$$

The force constant can be defined in terms of Hooke's Law. Alternatively, it may be defined in terms of the vibrational potential energy. The exerted force is equal to the

negative slope of the potential energy,  $F = -\frac{dV}{dq} = -fq$

$$\frac{dV}{dq} = fq$$

$$V = \int_{q=0}^q f q \, dq = \frac{f q^2}{2}.$$

Differentiating the potential energy twice with respect to  $q$ ,

$$f = \frac{d^2 V}{dq^2}.$$

The force constant is found to be equal to the second derivative of the potential energy.

In heteronuclear diatomic molecule, the reduced mass of the molecule is made from two atoms of masses, A and B is given by  $\frac{1}{\mu} = \frac{1}{m_A} + \frac{1}{m_B}$  and the frequency is

$$\nu = \frac{1}{2\pi} \sqrt{\frac{f}{\mu}}.$$

The use of the reduced mass ensures that the centre of mass of the molecule is not affected by the vibration. Only one vibrational frequency is allowed although all amplitudes are possible. In other words, the two particle system is mathematically identical to the one particle system, provided the reduced mass of the pair is used. Thus, these principles are still used in the treatment of polyatomic molecules. Assuming no energy is lost, the kinetic energy and the potential in a periodic form can be written as:

$$T = \frac{1}{2} m \left( \frac{dq}{dt} \right)^2 = \frac{f q_0^2}{2} \sin^2(2\pi \nu_0 t + \phi)$$

$$V = \frac{1}{2} f q^2 = \frac{f q_0^2}{2} \cos^2(2\pi \nu_0 t + \phi).$$

Total energy is constant,  $E = T+V = \frac{f q_0^2}{2}$ . The classical harmonic oscillator can have any amplitude and energy. This is quite different to the quantum mechanical harmonic oscillator which is discussed below.

### 3.3.3 The Quantum Mechanical Harmonic Oscillator

From the classical mechanics, the frequencies of vibrations may be calculated correctly. Quantum mechanics also provides greater insight into aspects other than the frequencies. Consider two masses by weightless springs as in the classical mechanics of

harmonic motion. The Hamiltonian operator for the harmonic oscillator problem is the classical total energy of the system [25].

$$H(q) = T(q) + V(q) \quad (16)$$

$$\begin{aligned} H &= \frac{1}{2} m_1 \dot{r}_1^2 + \frac{1}{2} m_2 \dot{r}_2^2 + \frac{1}{2} f q^2 \\ &= \frac{1}{2} \mu \dot{q}^2 + \frac{1}{2} f q^2 \end{aligned} \quad (17)$$

The quantum mechanical Hamiltonian operator is then,  $\hat{H} = -\frac{\hbar^2}{2\mu} \frac{d^2}{dq^2} + \frac{1}{2} f q^2$

The eigenvalues of this Hamiltonian are the energy levels:

$$E = \left( n + \frac{1}{2} \right) \frac{h}{2\pi} \sqrt{\frac{f}{\mu}}, \text{ where } n = \text{quantum number } 0, 1, 2, \dots, \infty.$$

There is only one quantum number allowed to change for each transition. Therefore,

the transition energy is given by  $\Delta E = \frac{h}{2\pi} \sqrt{\frac{f}{\mu}}$ . Since  $\Delta E = h\nu$ , the frequency associated

with the change is  $\nu = \frac{1}{2\pi} \sqrt{\frac{f}{\mu}}$ . It is shown that the result is the same as in classical

mechanics. In quantum mechanics,  $n=0$ , gives a finite energy, whereas, there is no analogue of the zero-point motion in the classical mechanics.

There are many possible vibrational levels within each electronic state at which they vibrate corresponding to energy levels. According to the Born-Oppenheimer and simple harmonic approximations, the vibrational frequencies are determined by the normal modes corresponding to the molecular electronic ground state potential energy surface. Thus, the vibrational frequencies are related to the strength of the bond and the masses of the atoms. The electronic levels usually occur in the visible region whereas the vibrational and rotational levels occur in the infra-red.

In simple molecules the spectra are clearly resolved. In contrast, more complex molecular structures will lead to more absorption bands which give a more complex and poorly resolved spectrum.

# CHAPTER 4

## Computerized Simulation of Magnetoresistance Random Access Memory Material ( $\text{Fe}_x\text{Ni}_y$ )

An alloy of Ni and Fe is proposed to be used as a random access memory material in computers and in data storage devices. The Ni and Fe atoms are simulated by using the density-functional theory. The vibrational frequencies of materials are calculated of variable ratio of Ni and Fe atoms and the anomalies in the concentration as a function of the largest vibrational frequency is observed.

### 4.1 Introduction

The modern computers use semiconductors for data storage. It is possible to replace these semiconductor films by a suitable magnetic material. An effort is being made to use the Ni-Fe alloy. The ratio of Ni and Fe metals in the alloy is not known. By means of computerized simulations, it may be possible to find the concentration of Ni in Fe for which the material works the best. Magnetic tunnel transistors are used to study spin-dependent transport in  $\text{Ni}_{81}\text{Fe}_{19}$  and  $\text{Co}_{84}\text{Fe}_{16}$  films [26]. The spin-polarized current can be much more efficient as a switch than the magnetic fields [27]. The film thickness and shape is important for the optimum hysteresis [28, 29].



The calculation of vibrational frequencies of clusters containing Ni and Fe atoms is reported. Since, the numbers of atoms are varied; the concentration of Ni in Fe is found for which the material has maxima or minima in the vibrational frequency.

## 4.2 Methodology

Density-functional theory in the local-density approximation (LDA) is used to calculate the vibrational frequencies of clusters of atoms. The details of the derivation are given by Lopez-Duran *et. al* [30]. The clusters of atoms are first optimized for the minimum energy. Then bond lengths and angles are determined for the stable configuration. The vibrational frequencies are calculated for the optimized clusters by using the double zeta spin polarized orbitals. The calculated clusters are then described.

## 4.3 Clusters of Ni<sub>x</sub>Fe<sub>y</sub> Atoms

- (i) NiFe. The diatomic linear molecule has a bond length of 2.1468 Å when double zeta wave functions are used and 2.1339 Å when polarized wave functions are used. The effect of spin polarization on the bond length is observed to be about 6 percent. Usually, the effect of magnetism on various thermodynamic properties is quite large. Hence, only the polarized double zeta wave functions are used. The vibrational frequency of Ni-Fe diatomic molecule is 312.7 cm<sup>-1</sup> for the unpolarized and 316.4 cm<sup>-1</sup> for the polarized wave functions, but the intensity is quite small, ~0.006 km/mol, indicating that the number of diatomic molecules formed is quite small. This is due to the strong Coulomb interactions in the metal.
- (ii) NiFe<sub>2</sub> (linear). The vibrations are generated in triatomic molecules which are more abundant than the diatomic molecules. The bond lengths in NiFe<sub>2</sub> molecule are Fe-Ni = 2.1376 Å and Fe-Fe = 4.2752 Å. It has a strong vibrational frequency at 302.7 cm<sup>-1</sup> with intensity 5.4 km/mole.

- (iii) NiFe<sub>2</sub> (triangular). In this molecule Fe-Ni = 2.2190 Å and Fe-Fe = 2.1919 Å. There is a strong vibrational frequency (intensity) at 253.5 cm<sup>-1</sup> (3.4 km/mole) and a weak line at 363.1 cm<sup>-1</sup> (0.007 km/mole).
- (iv) NiFe<sub>3</sub> (triangular). In this system the Fe atoms form a triangle and Ni sits in the centre of the triangle with distance Ni-Fe = 2.1573 Å and Fe-Fe = 3.731 Å. There is a strong vibration at 328.1 cm<sup>-1</sup> (2.5 km/mole).
- (v) NiFe<sub>3</sub> (pyramidal). In this cluster, three Fe atoms form a triangle and one Ni atom sits on top position. The distance Fe-Ni = 2.3675 Å and Fe-Fe distance is 2.190 Å. The vibrational frequencies (intensities) calculated from the first principles with polarized orbitals are, 125.5 (1.5), 231.1 (11.3), 252.2 (12.4) and 360.5 (26.4) in units of cm<sup>-1</sup> (km/mole). The vibrational spectrum calculated from the first principles is shown in Figure 4.3.1.

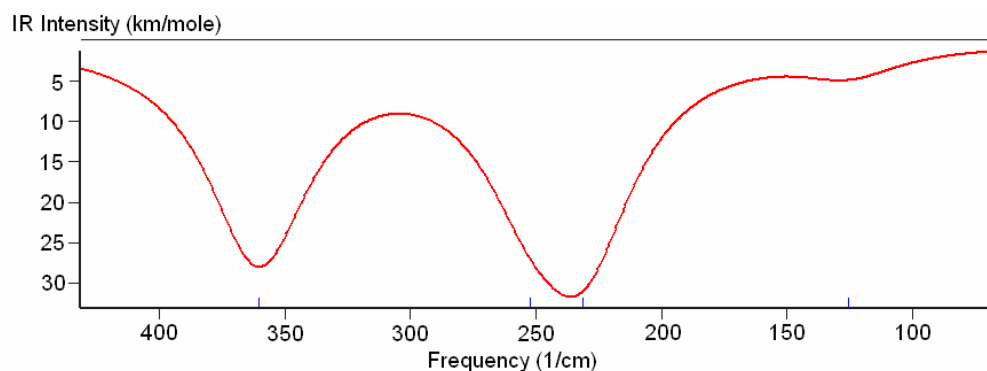


Figure 4.3.1. The vibrational spectrum of NiFe<sub>3</sub> (pyramidal) calculated with polarized orbitals.

- (vi) NiFe<sub>4</sub> (square). In this cluster four Fe atoms are on the four corners of a square and Ni is in the centre of the square. The bond distances are, Fe-Ni = 2.0946 Å and Fe-Fe = 2.962 Å. The strong vibrational mode is found at 377.3 (2.5) cm<sup>-1</sup> (km/mole).
- (vii) NiFe<sub>4</sub> (pyramidal). This molecule has four Fe atoms on a square and one Ni atom is on the top position with distances, Fe-Ni = 2.3447 Å, Fe-Fe = 2.073 Å. The vibrational frequencies (intensities) are found to be 163.9 (0.002), 263.9 (3.8), 342.5 (0.44), 394.9 (0.0005) cm<sup>-1</sup> (km/mole).

(viii) NiFe<sub>4</sub> (Td). One Ni atom is in the centre and four Fe atoms form a tetrahedron. The bond lengths are Fe-Ni = 2.093 Å and Fe-Fe = 3.419 Å. A very strong vibrational mode occurs at 369.8 cm<sup>-1</sup> with degeneracy of three.

The highest frequency of these eight clusters as a function of number of Fe atoms is examined. With one atom the largest frequency is 316.4 cm<sup>-1</sup>, with two atoms it is 363.1 cm<sup>-1</sup>, with three atoms 360.5 cm<sup>-1</sup> and with four atoms is 377.3 cm<sup>-1</sup>. Taken as a whole, the trend of the function shows that the largest frequency increases with increasing number of Fe atoms. No particular peak is found. For n = 1, the frequency is small and for n = 4 it is large. There is approximately a plateau between n = 2 and 3. Hence the properties of the alloy near n = 2 or 3 are different from that near n = 1 or 4. The alloy of formula NiFe<sub>2</sub> is therefore different from those of other concentrations. The following clusters are made with two Ni atoms and the numbers of Fe atoms are varied.

(ix) Ni<sub>2</sub>Fe (linear). In this system the distances are Fe-Ni = 2.2701 Å and Ni-Ni = 4.540 Å, and there is a strong vibrational peak at 267.1 (3.4) cm<sup>-1</sup> (km/mole).

(x) Ni<sub>2</sub>Fe (triangular). In this molecule the bond lengths are Fe-Ni = 2.1753 Å and Ni-Ni = 2.256 Å. The vibrational frequencies (intensities) are 134.36 (43.1), 222.6 (1.8) and 361.6 (0.02) cm<sup>-1</sup> (km/mole).

(xi) Ni<sub>2</sub>Fe<sub>2</sub> (rectangular). The alternate atoms are Ni and Fe with bond distances Fe-Ni = 2.1647 Å, Ni-Ni = 2.887 Å and Fe-Fe = 3.248 Å. The strong vibrational frequencies (intensities) are found at 63.6 (0.09), 282.2 (0.59) and 294.2 (4.7) cm<sup>-1</sup> (km/mole). The dipole strengths of these modes are 6.13, 8.4 and 63.5 esu respectively.

(xii)  $\text{Ni}_2\text{Fe}_3$  (bipyramidal). The three Fe atoms form a triangle and two Ni atoms sit on each side of the triangle. The Fe-Fe distance is 2.291 Å, Ni-Ni distance is 3.844 Å and Fe-Ni distance is 2.3332 Å. The vibrational frequencies (intensities) {degeneracies} are 121.3 (0.8) {2}, 247.1 (8.3) and 323.5 (0.45)  $\text{cm}^{-1}$  (km/mole). The vibrational spectrum calculated from the first principles is given in Figure 4.3.2.

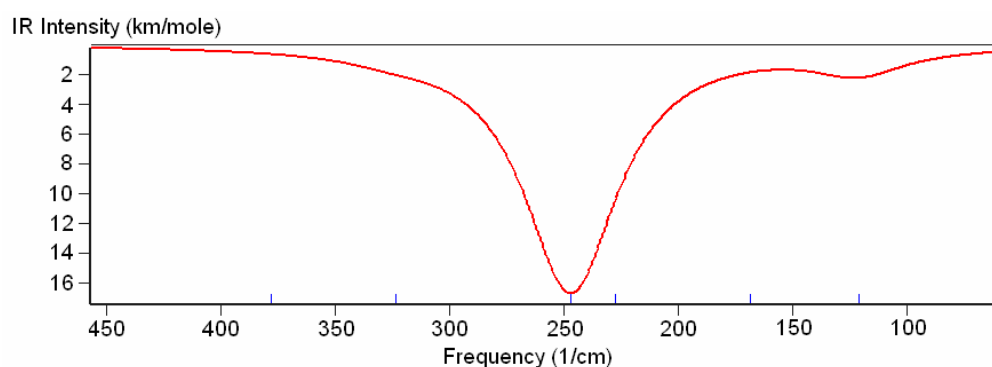


Figure 4.3.2. Vibrational spectrum of  $\text{Ni}_2\text{Fe}_3$  (bipyramidal) calculated from the first principles.

(xiii)  $\text{Ni}_2\text{Fe}_4$  (bipyramidal). The four Fe atoms form a square and two Ni atoms sit on each side of the square. The Ni-Ni distance is 3.663 Å, Fe-Fe distance is 2.1028 Å and the Fe-Ni distance is 2.3591 Å. The calculated vibrational frequencies (intensities) {degeneracies} are 136.5 (2.17) {2}, 299.4 (2.36), 320.3 (1.69) {2}  $\text{cm}^{-1}$  (km/mole).

The largest vibrational frequency for  $\text{Ni}_2\text{Fe}_n$  is 267.1 ( $n = 1$ ), 294.2 ( $n = 2$ ), 323.5 ( $n = 3$ ) and 320.3 ( $n = 4$ ). Although the frequency increases from  $n = 1$  to  $n = 2$ , it is almost flat near  $n = 3$  or 4. Hence, the flatness in the vibrational frequency for this concentration may indicate special physical properties and for this concentration.

(xiv)  $\text{Ni}_3\text{Fe}$  (triangular). In this cluster the three Ni atoms form a triangle and Fe atom is in the centre. The bond lengths are, Fe-Ni = 2.0723 Å and Ni-Ni = 3.589 Å. The

strong vibrational frequencies (intensities) {degeneracies} are, 83.9 (1.7) {2} and 404.1 (5.2) {2}  $\text{cm}^{-1}$  (km/mole).

(xv)  $\text{Ni}_3\text{Fe}_2$  (bipyramidal). The three Ni atoms form a triangle and two Fe atoms are on each side of the triangle to form a bipyramid. The bond distances are, Fe-Ni = 2.3414 Å, Ni-Ni = 2.3044 Å and Fe-Fe = 3.853 Å. The strong vibrational frequencies (intensities) {degeneracies} are as follows: 141.7 (0.5) {2}, 237.2 (1.5) {2} and 277.5 (4.3)  $\text{cm}^{-1}$  (km/mole).

(xvi)  $\text{Ni}_3\text{Fe}_3$  (hexagonal). The Ni and Fe atoms are on alternate sites. The bond lengths are, Fe-Ni = 2.1566 Å, Ni-Ni = 3.372 Å and Fe-Fe = 4.015 Å. The strong vibrational frequencies (intensities) {degeneracies} are 112.5 (0.9), 257.6 (10.7) {2} and 319.1 (1.1) {2}  $\text{cm}^{-1}$  (km/mole).

(xvii)  $\text{Ni}_3\text{Fe}_3$  (triangle inside triangle). Fe atoms form a large triangle and Ni atoms form a small triangle such that the smaller triangle fits perfectly inside the bigger triangle. The Fe-Ni-Fe forms the sides of the triangle. The distances are Fe-Ni = 2.2387 Å, Ni-Ni = 2.3069 Å and Fe-Fe = 4.477 Å. The strong vibrational frequencies (intensities) {degeneracies} are 147.8 (0.18) {2}, 193.1 (2.7) {2}, 333.4 (5.9) {2}  $\text{cm}^{-1}$  (km/mole).

In the above four clusters the largest frequency reduces as a function of n in  $\text{Ni}_3\text{Fe}_n$  only for n going from 1 to 2 but at n = 3 a large value is obtained. Hence n = 2 maybe indicating unique physical properties.

(xviii)  $\text{Ni}_4\text{Fe}$  (pyramidal). In this system four Ni atoms form a square and one Fe sits on top position. The Ni-Ni distance is 2.3231 Å and Fe-Ni distance is 2.2319 Å. The vibrational frequencies (intensities) {degeneracies} are, 132.1 (2.1) {2}, 188.3 (4.6), 291.2 (4.1) {2} and 358.9 (2.8)  $\text{cm}^{-1}$  (km/mole).

(xix)  $\text{Ni}_4\text{Fe}$  (planar). In this cluster the Ni ions are on the corners of a square and Fe is in the centre. The bond distances are Fe-Ni = 2.0649 Å and Ni-Ni = 2.920 Å. There is a strong vibration at 408.9  $\text{cm}^{-1}$ .

(xx)  $\text{Ni}_4\text{Fe}_2$  (bipyramidal). The four Ni form a square and two Ni atoms sit one on each side of the square. The bond distances are Fe-Ni = 2.3160 Å, Ni-Ni = 2.3256 Å and Fe-Fe = 3.262 Å. The strong vibrational frequencies (intensities) {degeneracies} are, 152.9 (0.1) {2}, 274.6 (3.0) and 291.9 (3.6) {2}  $\text{cm}^{-1}$  (km/mole).

(xxi)  $\text{Ni}_4\text{Fe}_3$  (boat shape). The four Ni form a rectangle with one Fe in the centre as well as one Fe on left side of the rectangle and another Fe on the right hand side of the rectangle. The bond distances are Fe-Ni = 2.2709 Å, Ni-Ni = 2.4145 Å and Fe-Fe = 3.195 Å. The vibrational frequencies (intensities) {degeneracies} are as follows 68.1 (0.1), 99.2 (1.5), 102.2 (1.4), 105.9 (2.0), 139.8 (2.9), 237.1 (0.9), 242.2 (0.17), 266.3 (0.9), 309.1 (1.6), 323.8 (10.8) and 330.6 (2.1)  $\text{cm}^{-1}$  (km/mole). The vibrational spectrum calculated from the first principles is shown in Figure 4.3.3.

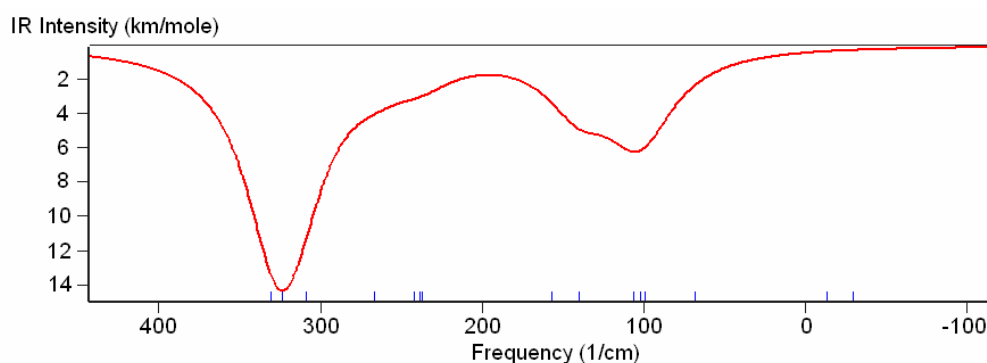


Figure 4.3.3. The vibrational spectrum calculated from the first principles using polarized orbitals of  $\text{Ni}_4\text{Fe}_3$  (boat shape).

(xxii)  $\text{Ni}_4\text{Fe}_4$  (deformed cube). The two Ni atoms and two Fe atoms form a rectangle and then one more layer of four atoms is put on top so that Ni is on top of Ni and Fe is on top of Fe. The bond distances are Fe-Ni = 2.2926 Å, Ni-Ni = 2.2983 Å and Fe-Fe = 2.526 Å. The vibrational frequencies (intensities) {degeneracies} are,

135.8 (0.07), 157.8 (0.003), 192.5 (3.1), 235.6 (2.8), 267.7 (6.1) and 291.6 (0.09)  $\text{cm}^{-1}$  (km/mole).

(xxiii)  $\text{Ni}_4\text{Fe}_4$  (square inside square). The Ni atoms form a small square and Fe forms a large square. The inside square is rotated 90 degrees with respect to the outer square. The bond distances are, Fe-Ni = 2.2184 Å, Ni-Ni = 2.306 Å and Fe-Fe = 4.313 Å. The positive frequencies (intensities) are, 127.48 (0.1), 128.5 (0.1), 144.8 (0.2), 145.2 (0.007), 199.2 (0.0001), 216.8 (0.00002), 223.7 (5.1), 229.7 (5.86), 298.3 (19.8), 299.6 (10.1), 307.1 (0.008) and 365.1 (0.16)  $\text{cm}^{-1}$  (km/mole).

In the series  $\text{Ni}_4\text{Fe}_n$  apparently there is a minimum at  $n = 2$  and the vibrational frequencies again shoot up at  $n = 4$  but yet it depends on the structure. The material compositions as well as the structures play an important role in determining the material with special properties.

## 4.4 Conclusions

Several clusters of FeNi atoms are made and the vibrational frequencies are calculated. From the largest vibrational frequencies, plateaus in the frequencies as a function of concentration are observed for each  $\text{NiFe}_n$ ,  $\text{Ni}_2\text{Fe}_n$ ,  $\text{Ni}_3\text{Fe}_n$  and  $\text{Ni}_4\text{Fe}_n$ . Hence, these materials may have special physical properties. Currently, these calculations are waiting to be proven experimentally. In this way, a method is found to find concentration of the constituent atoms which may be important. The present material is of significant importance as a candidate for memory material.

# CHAPTER 5

## DFT Calculation of Vibrational Frequencies of FeCoB m-RAM

The present available random access memory materials are semiconductors. It is proposed to develop magnetoresistance based random access memory (m-RAM) materials. Hence, an alloy of Fe, Co and B is considered which will be strongly magnetic and work well as a memory device. The vibrational frequencies of clusters of atoms of Fe, Co and B are calculated. The larger vibrational frequencies indicate larger force constants,  $\nu = \frac{1}{2\pi} \sqrt{\frac{f}{\mu}}$ . FeCoB<sub>2</sub> is found to have the largest vibrational frequency of 869.5 cm<sup>-1</sup> whereas BFeCo<sub>2</sub> has 502.59 cm<sup>-1</sup>. The ratio of constituents and the structures which have large force constant are identified. Hence, FeCoB<sub>2</sub> is better than BFeCo<sub>2</sub>. The cluster formation depends on the method of quenching. Hence, method of preparation can be modified to achieve large force constants.

### 5.1 Introduction

The transfer of spin angular momentum from a spin polarized current to a small ferromagnet can switch the orientation of the ferromagnet. This process can be faster than that produced by a current generated magnetic field. The semiconductors are therefore distinguished from the magnetic materials. The spin in a ferromagnet may



switch faster than non-polarized semiconductors [27]. Hence, there is a need to develop magnetic random access memory devices (MRAM). These magnetic devices depend on the shape of the material [29] and naturally on the composition. Hence, the ratios of various magnetic atoms are of interest such as Fe and Co in the magnetic material made from FeCoB.

In this chapter, many clusters of varying number of Fe and Co atoms are made to determine which ratio will work the best. The vibrational frequencies of the clusters are determined which can be used to indicate the force constant. Hence, the ratio of Fe: Co for which the force constant is optimum can be determined. Density functional theory is used to calculate the vibrational frequencies of clusters of atoms which are used to find the material for which the force constant is optimum.

## 5.2 Methodology

The density-functional theory is obtained by writing the Hamiltonian in the form of electron density,

$$\rho(\vec{r}) = \langle \Psi | \hat{\rho}(\vec{r}) | \Psi \rangle = \left\langle \Psi \left| \sum_{\sigma} \hat{\psi}_{\sigma}^{\dagger}(\vec{r}) \hat{\psi}_{\sigma} \right| \Psi \right\rangle = N \sum_{\sigma} \int |\Psi(\vec{r}, \sigma, x_2, \dots, x_N)|^2 dx_2 \dots dx_N \quad (18)$$

where,  $dx$  denotes integration over the spatial variable  $\vec{r}$  and summation over the spin variable  $\sigma$ . The density usually depends on the coordinates,  $n(x)$ . Hence, the differential of the Hamiltonian with respect to coordinate dependent density leads to a functional Kohn-Sham equation [19, 31, 32, 33]. Along with this equation and the motion of nuclei and can be used to determine vibrational frequencies. Our experience with this type of calculation [34-36] shows that the predicted vibrational frequencies are quite close to the experimental values. The Amsterdam density functional programme (ADF) is used to calculate the vibrational frequencies.

### 5.3 Clusters of Atoms

- (i) FeCoB (linear). The configurations of atoms are optimized for which the energy is a minimum. For the linear molecule FeCoB, the bond lengths found by using double-zeta wave functions are Fe-Co = 206.9 pico meter, Co-B = 192.2 pm and Fe-B = 399.1 pm. The values are sensitive to the choice of wave functions. For non-magnetic atoms, the double-zeta wave function works the best as far as obtaining agreement with the experimental data is concerned. In the case of Fe and Co which have strong magnetic moment, is observed that by using the spin polarized double zeta wave functions (DZP) it gave slightly different values where Fe-Co = 207.0 pm, Co-B = 189.8 pm and Fe-B = 396.8 pm. The distance of Co-B with 189.8 pm found for the polarized double zeta wave functions (DZP) is to be compared with 192.2 pm found from unpolarized wave functions. The values differ by about 2 percent. Hence, in this chapter, the values given are calculated by using DZP wave functions. In the molecule Fe-Co-B, one of the frequencies is due to Fe-Co bond and the other is due to Co-B bond. The values of the vibrational frequencies (intensity) found are 267.0 (10.1) and 542.5 (13.8) in units of  $\text{cm}^{-1}$  (km/mole).
- (ii) Co-Fe-B (linear). In the previous cluster Co was in the centre while in the present case, Fe is in the centre. The forces are dependent on the geometric position of the atoms and on the electronic configuration which is at the end of the molecule. The DZP wave functions for this system gave the bond lengths, Fe-Co = 218.5 pm, Co-B = 387.7 pm and Fe-B = 169.1 pm. The vibrational frequencies (intensity) are  $247.3 \text{ cm}^{-1}$  (0.61) and  $755.1 \text{ cm}^{-1}$  (0.39) in units of  $\text{cm}^{-1}$  (km/mole).
- (iii) Fe-B-Co (linear). In this molecule B atom is in the centre. The DZP optimized bond lengths are Fe-Co = 351.9 pm, Co-B = 171.5 pm and Fe-B = 180.4 pm. The calculated vibrational frequencies (intensities) {degeneracy} are, 194.97 (40) {2}, 286.84 (2.3) and  $912.26 (17.7) \text{ cm}^{-1}$  (km/mole).

(iv) FeCoB (triangular). In this configuration, the DZP optimized bond lengths are Fe-Co = 208.6 pm, Co-B = 181.2 pm and Fe-B = 182.1 pm. The vibrational frequencies (intensities) are 324.0 (2.4), 384.7 (16.7) and 764.1 (17.5)  $\text{cm}^{-1}$  (km/mole).

The largest vibrational frequency indicates that the geometrical configuration plays an important role. When boron atom is in the centre, the largest vibrational frequency is obtained. This largest frequency is also associated with the largest force constant.

(v) BFeCoB (linear). The linear molecule is made with the atoms in the same sequence as indicated. In this case the bond lengths calculated by DZP wave functions are found to be Fe-Co = 246.1 pm, Co-B = 167.8 pm, Fe-B = 169.2 pm and B-B = 583.1 pm. The vibrational frequencies are 98.35 (3.29) {2}, 173.4 (0.001), 768.54 (0.14) and 803.6 (0.07)  $\text{cm}^{-1}$  (km/mole) {degeneracy}.

(vi) CoFeB<sub>2</sub> (triangular). The atoms CoB<sub>2</sub> form a triangle and Fe is located in the centre of the triangle. In this case the bond lengths found are Fe-Co = 208.1 pm, Co-B = 173.3 pm, Fe-B = 367.3 pm and B-B = 180.4 pm. The vibrational frequencies calculated are 217.09 (20.6), 346.2 (82), 693.5 (0.52) and 810.9 (7.9)  $\text{cm}^{-1}$  (km/mole). The calculated spectrum is shown in Figure 5.3.1.

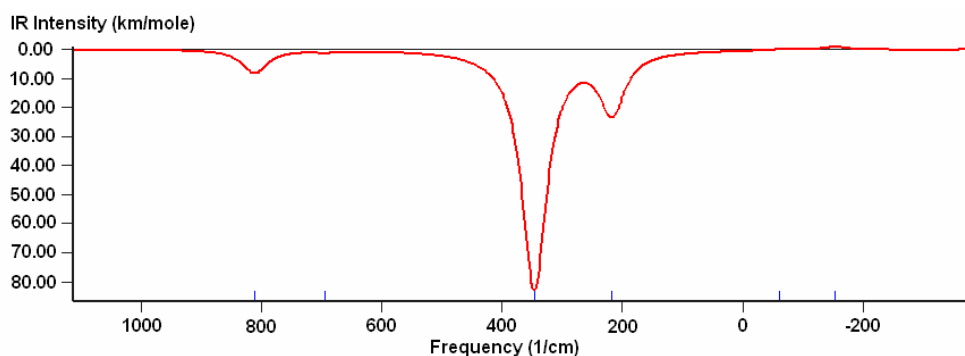


Figure 5.3.1. Vibrational spectrum of CoFeB<sub>2</sub> (triangular) calculated from the first principles.

(vii)  $\text{FeCoB}_2$  (triangular). The  $\text{FeB}_2$  form a triangle with Co in the centre of the triangle.

The bond lengths are calculated to be Fe-Co = 217.7 pm, Co-B = 177.0 pm, Fe-B = 382.6 pm and B-B = 169.7 pm. The vibrational frequencies calculated are found to be 224.6 (7.5), 500.1 (1.4), 632.8 (0.3), and 869.5 (0.02). The calculated vibrational spectrum is shown in Figure 5.3.2.

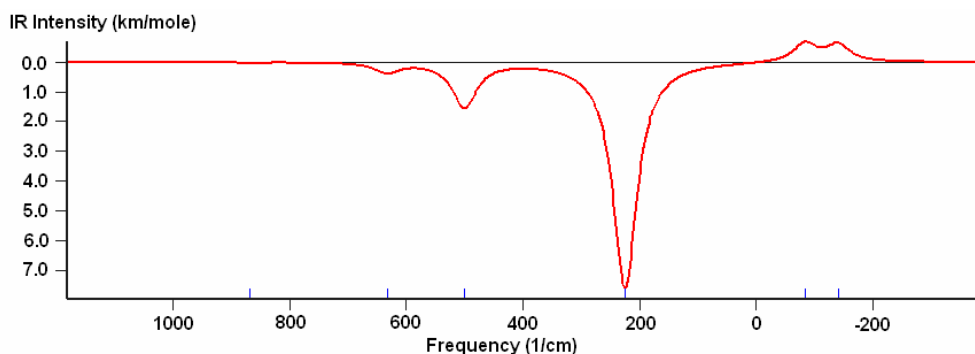


Figure 5.3.2. Spectrum of  $\text{FeCoB}_2$  (triangular) calculated using DZP wave functions.

(viii)  $\text{FeCo}_2\text{B}$  (triangular). The  $\text{FeCo}_2$  form a triangle and B is located in the centre. The

bond distances are found to be Fe-B = 181.8 pm, B-Co = 185.0 pm, Co-Co = 208.1 pm and Fe-Co = 350.5 pm. The vibrational frequencies (intensities) found are 130 (30), 232.0 (0.3), 360.6 (0.009), 418.5 (11.4) and 813.9 (70)  $\text{cm}^{-1}$  (km/mole). The calculated vibrational spectrum is shown in Figure 5.3.3.

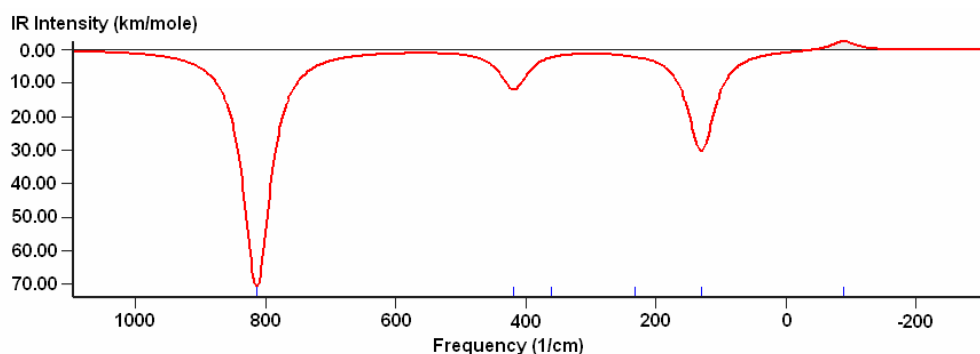


Figure 5.3.3. Vibrational spectrum of  $\text{FeCo}_2\text{B}$  (triangular).

(ix)  $\text{BFeCo}_2$  (triangular). The atoms  $\text{BCo}_2$  form a triangle and Fe is located in the centre.

The DZP bond lengths are B-Fe = 207.3 pm, Fe-Co = 222.9 pm, Co-Co = 214.8 pm and Co-B = 416.8 pm. The calculated vibrational frequencies (intensities) are, 22.2 (0.65), 50.1 (1.8), 218.9 (0.48), 228.1 (3.38), 347.1 (1.5) and 502.6 (0.32)  $\text{cm}^{-1}$  (km/mole). The vibrational spectrum calculated for this molecule is given in

Figure 5.3.4.

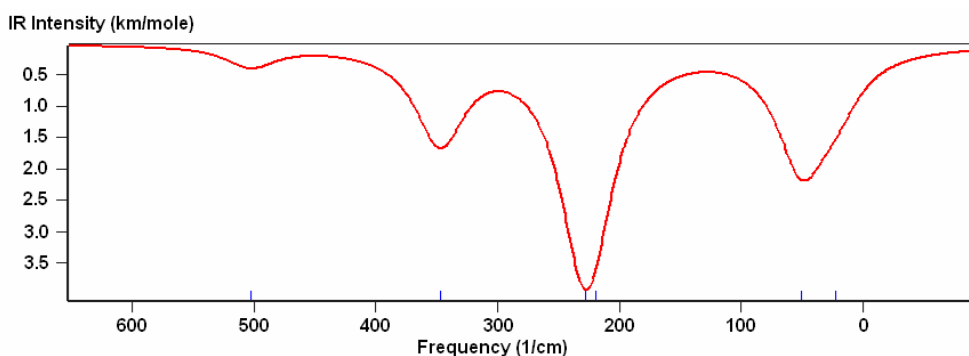


Figure 5.3.4. The vibrational spectrum of  $\text{BFeCo}_2$  (triangular) calculated with polarized orbitals.

(x)  $\text{CoBFe}_2$  (triangular). The atoms  $\text{CoFe}_2$  are on the corners of a triangle and B is in the centre. The DZP bond lengths are Co-B = 182.8 pm, B-Fe = 189.1 pm and Fe-Fe = 202.0 pm. The vibrational frequencies (intensities) are 128.3 (31), 221.2 (1.8), 351.2 (11), 396.9 (6.8) and 880.4 (8.2)  $\text{cm}^{-1}$  (km/mole). The vibrational spectrum calculated from the first principles DFT (LDA) is given in Figure 5.3.5.

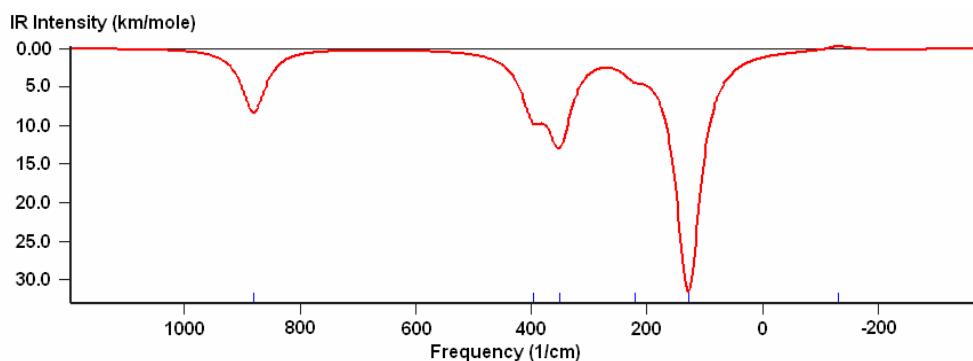


Figure 5.3.5. The vibrational spectrum of  $\text{CoBFe}_2$  (triangular) calculated from the first principles by using polarized orbitals.

(xi) B-Co-B-Fe (rectangular). In this molecule the two B atoms are on two opposite corners of a distorted rectangle. The Co and Fe atoms are on the remaining corners. The bond lengths are Fe-Co = 252.6 pm, Co-B = 177.7 pm, Fe-B = 177.0 pm and B-B = 249.1 pm. The vibrational frequencies (intensities) are 288.8 (1.9), 569.1 (3.6), 686.9 (5.0), 751.7 (100) and 767.8 (2.2)  $\text{cm}^{-1}$  (km/mole). The calculated vibrational spectrum is shown as in Figure 5.3.6.

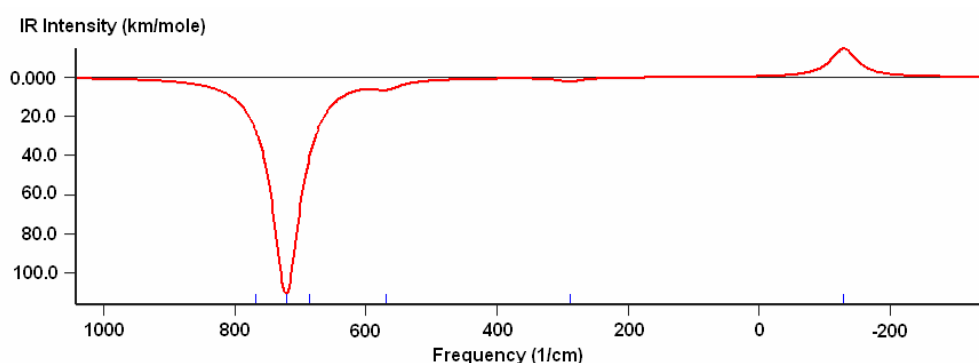


Figure 5.3.6. Spectrum of B-Co-B-Fe (rectangular) calculated by using DZP wave functions.

(xii)  $\text{FeCo}_2\text{B}$  (rectangular). The Co atoms are on opposite corners of a distorted rectangular shaped molecule. The Fe and B are also on the opposite corners. The bond lengths are B-Co = 176.0 pm, Fe-Co = 211.7 pm, Co-Co = 308.2 pm and Fe-B = 230.2 pm. The calculated vibrational frequencies (intensities) are found to be 114.8 (14.7), 178.7 (7.3), 284.3 (0.87), 311.6 (0.07), 585.9 (2.4) and 811.6 (30.4)  $\text{cm}^{-1}$  (km/mole). The calculated vibrational spectrum is given in Figure 5.3.7.

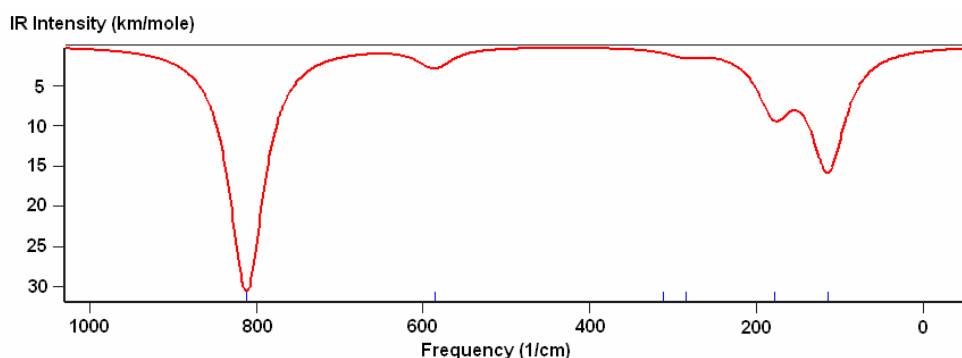


Figure 5.3.7. Vibrational spectrum of  $\text{FeCo}_2\text{B}$  (rectangular).

(xiii)  $\text{Fe}_2\text{CoB}$  (distorted rectangular). The  $\text{Fe}_2$  atoms are on the opposite corners of a distorted rectangle and the B and Co are also on the opposite corners of the rectangle. The bond lengths are Co-B = 196.8 pm, Co-Fe = 220.1 pm and Fe-B = 182.2 pm. The calculated vibrational frequencies (intensities) are 116.6 (16.7), 198.2 (1.0), 235.1 (0.92), 272.7 (0.22), 602.2 (4.7) and 708.6 (26.8)  $\text{cm}^{-1}$  (km/mole). The vibrational spectrum calculated from the first principles is given in Figure 5.3.8.

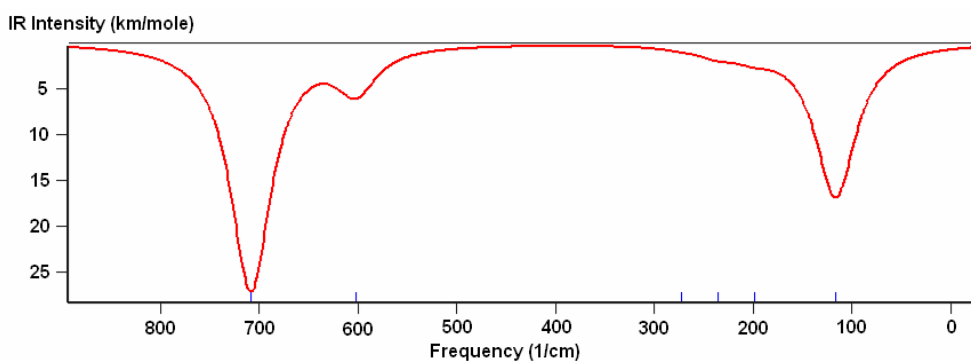


Figure 5.3.8. Vibrational spectrum of  $\text{Fe}_2\text{CoB}$  (distorted rectangular) calculated using DZP wave functions.

## 5.4 Conclusions

Out of all of the clusters of atoms studied above, the linear configuration Fe-B-Co with B in the centre gave the highest frequency of  $912.26 \text{ cm}^{-1}$ . Hence, the linear material has the strongest force constant. The triangular  $\text{BFeCo}_2$  with Fe in the centre has the smallest vibrational frequency of  $502.6 \text{ cm}^{-1}$ . Hence, it is possible to distinguish the memory material for optimum memory performance.

# CHAPTER 6

## Large Clusters

Clusters of atoms of Fe, Co and B have been made by using the density-functional theory in the local density approximation (LDA). The structural parameters, such as bond lengths and vibrational frequencies have been obtained by using the double zeta (DZ) wave functions as well as with spin polarized orbitals (DZP). Since materials of MRAM are ferromagnetic, effect of magnetism is large. Thus, only the spin polarized values are considered in this study.

### 6.1 Introduction

The clusters of atoms containing 3 to 4 atoms each are given in the previous chapters. In the present chapter, the clusters containing 5 or more atoms are discussed. Model 1 contains clusters with 5 atoms, model 2 has clusters of 6 atoms, model 3 has clusters of 7 atoms, model 4 has clusters of 8 atoms... model 7 has clusters of 11 atoms each. The largest frequency in each clusters are examined.

### 6.2 Computational Results

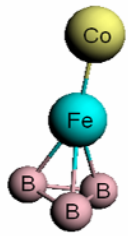
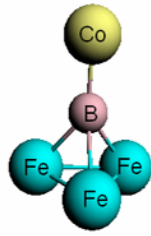
#### 6.2.1 Model 1

Model 1 consists of clusters with 5 atoms. Different structure and combination atoms of five are built. For cluster  $\text{FeCoB}_3$ , the bond distance among boron atoms is 169.0 pm,



Fe-Co is 211.0 pm and Fe-B is 217.5 pm. While, the bond distance among iron atoms is 201.9 pm, B-Co is 179.0 pm and B-Fe is 222.9 pm for cluster  $\text{Fe}_3\text{CoB}$  as shown below.

Table 6.2.1.1. Frequencies and intensities of clusters  $\text{FeCoB}_3$  and  $\text{Fe}_3\text{CoB}$  calculated using DZ wave functions.

 $\text{FeCoB}_3$		 $\text{Fe}_3\text{CoB}$	
Frequency ( $\text{cm}^{-1}$ )	Intensity (km/mole)	Frequency ( $\text{cm}^{-1}$ )	Intensity (km/mole)
-89.3	(-2.2)	-29.6	(-0.9)
169.3	(0.8)	213.3	(0.9)
268.3	(22.2)	235.8	(0.1)
409.0	(4.3)	219.0	(16.3)
703.6	(2.4)	385.2	(8.4)
933.0	(50.8)	825.5	(16.5)

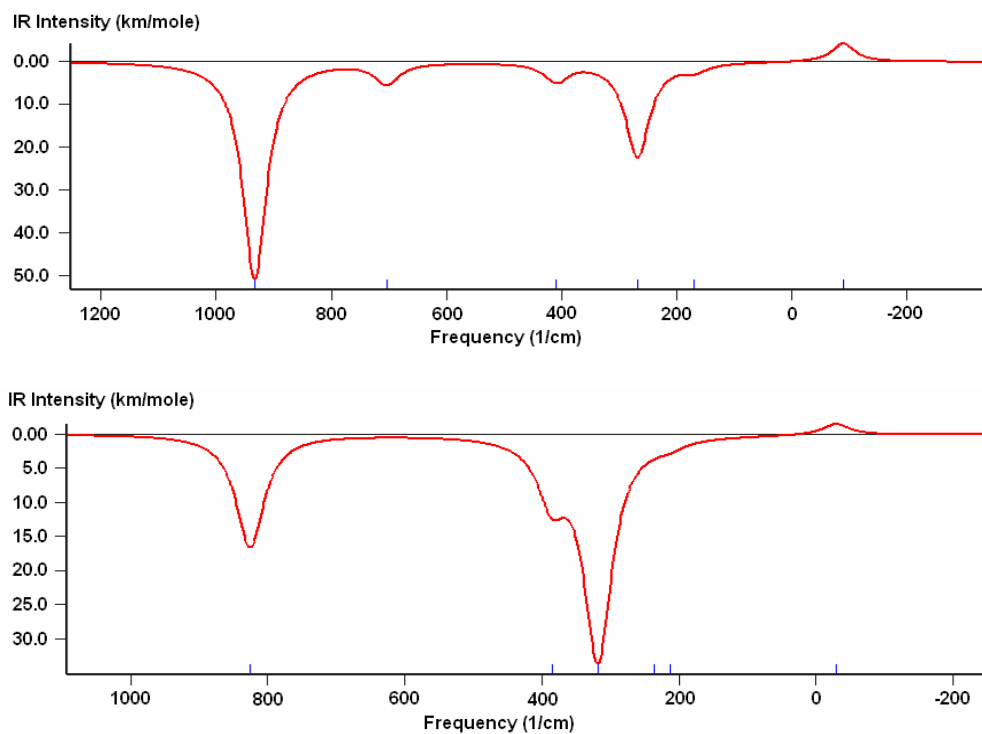


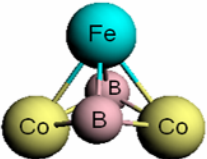
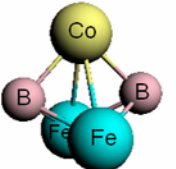
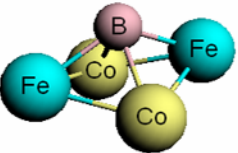
Figure 6.2.1.1. The first spectrum on top and the second spectrum shows peaks of  $\text{FeCoB}_3$  and  $\text{Fe}_3\text{CoB}$  respectively calculated using double zeta polarized orbitals.

Clusters of  $\text{FeCo}_2\text{B}_2$ ,  $\text{Fe}_2\text{CoB}_2$  and  $\text{Fe}_2\text{Co}_2\text{B}$  formed a distorted pyramid. Pictures and bond lengths of these clusters are shown in Table 6.2.1.2. The calculated vibrational frequencies (intensities) units of  $\text{cm}^{-1}$  (km/mole) using spin polarized orbitals for cluster  $\text{FeCo}_2\text{B}_2$  are 87.4 (0.5), 159.1 (0.1), 327.9 (1.2), 385.7 (0.7), 482.1 (40.7), 521.2 (34.9), 644.2 (8.6) and 760.8 (2.0).

Cluster  $\text{Fe}_2\text{CoB}_2$  shows two strong peaks at  $458.3 \text{ cm}^{-1}$  and  $568.7 \text{ cm}^{-1}$  with intensity of 56.4 km/mole and 63.1 km/mole respectively. There are six weak peaks where the frequencies (intensities) are 140.7 (0.0004), 183.7 (0.02), 321.1 (0.5), 465.9 (0.0006), 668.9 (16.6) and 738.4 (0.2) with units  $\text{cm}^{-1}$  (km/mole).

Vibrational frequencies of cluster  $\text{Fe}_2\text{Co}_2\text{B}$  shows one strong peak at  $432.4 \text{ cm}^{-1}$  (23.9 km/mole) with weak peaks,  $\text{cm}^{-1}$  (km/mole), at 96.9 (0.05), 188.1 (0.6), 198.8 (0.3), 245.0 (2.5), 263.9 (0.2), 590.6 (4.1) and 627.8 (5.5).

Table 6.2.1.2. Structures and bond lengths of clusters  $\text{FeCo}_2\text{B}_2$ ,  $\text{Fe}_2\text{CoB}_2$  and  $\text{Fe}_2\text{Co}_2\text{B}$ .

Cluster	Structure	Bond lengths (pm)
$\text{FeCo}_2\text{B}_2$		Fe-B = 188.2 Fe-Co = 228.8 Co-B = 186.6
$\text{Fe}_2\text{CoB}_2$		Co-Fe = 242.3 Co-B = 185.3 B-Fe = 188.8
$\text{Fe}_2\text{Co}_2\text{B}$		B-Co = 191.3 B-Fe = 193.0 Fe-Co = 224.2

The clusters  $\text{FeCoB}_3$ ,  $\text{FeCo}_3\text{B}$  and  $\text{Fe}_3\text{CoB}$  formed a symmetric structure of bipyramidal where three similar atoms form a triangle in middle and the atoms sit on each side of the triangle. The bond lengths in cluster  $\text{FeCoB}_3$  are B-B = 180.4 pm, Fe-B

= 182.1 pm and Co-B = 185.7 pm. The frequencies (intensities) {degeneracy} values are 324.9 (12.2) {2}, 359.0 (0.2), 577.9 (0.0003) {2}, 647.0 (5.6) {2}, 714.1 (23.5) and 858.0 (1.7) in units  $\text{cm}^{-1}$  (km/mole).

The bond lengths for the cluster  $\text{FeCo}_3\text{B}$  are 240.9 pm for Co-Co bond, 184.4 pm for Co-B bond and 221.7 pm for Fe-Co bond. The strongest peak appears at  $500.6 \text{ cm}^{-1}$  (24.6 km/mole) with degeneracy of two. The weak peaks appear to be 83.2 (0.3) {2}, 216.2 (1.6) {2}, 226.6 (4.8), 355.6 (0.002) and 694.7 (16.1), units of  $\text{cm}^{-1}$  (km/mole).

For cluster  $\text{Fe}_3\text{CoB}$ , there are three strong peaks with three weak peaks. The strong peaks are  $223.4 \text{ cm}^{-1}$  (6.7 km/mole),  $485.6 \text{ cm}^{-1}$  (16.9 km/mole) and  $714.0 \text{ cm}^{-1}$  (14.1 km/mole). While the weak peaks are at  $125.7 \text{ cm}^{-1}$  (km/mole),  $251.6 \text{ cm}^{-1}$  (3.1 km/mole) and  $365.7 \text{ cm}^{-1}$  (0.8 km/mole). The bond distances are Fe-Fe = 231.7 pm, Fe-Co = 224.6 pm and Fe-B = 188.7 pm.

## 6.2.2 Model 2

Three clusters with chemical composition of  $\text{FeCoB}_4$ ,  $\text{FeCo}_4\text{B}$  and  $\text{Fe}_4\text{CoB}$  forms bipyramidal structure. Four of the similar atoms form a square in middle with different atoms on each side. The structure of  $\text{FeCoB}_4$  gives the strongest peak at  $737.9 \text{ cm}^{-1}$  with intensity of 91.1 km/mole and weak peaks with frequencies (intensities) {degeneracy} at 243.7 (0.4) {2}, 376.1 (0.05), 492.0 (0.3) {2}, 679.4 (10.3) {2} and 938.6 (0.8). The bond distances for B-B = 169.9 pm, Fe-B = 188.7 pm and Co-B = 190.1 pm.

The bond lengths in cluster  $\text{FeCo}_4\text{B}$  are Co-Co = 223.1 pm, Fe-Co = 233.6 pm and Co-B = 193.0 pm. The vibrational frequencies are  $135.4 \text{ cm}^{-1}$ ,  $235.8 \text{ cm}^{-1}$ ,  $273.4 \text{ cm}^{-1}$ ,  $339.5 \text{ cm}^{-1}$ ,  $510.1 \text{ cm}^{-1}$  and  $622.4 \text{ cm}^{-1}$  with intensities of 0.2 km/mole, 5.2 km/mole, 1.8 km/mole, 0.8 km/mole, 15.1 km/mole and 14.3 km/mole respectively.

The cluster  $\text{Fe}_4\text{CoB}$  having frequencies (intensities) at 168.7 (0.7) {2}, 243.5 (3.8), 279.0 (3.1) {2}, 337.5 (0.03), 470.5 (24.1) {2} and 589.6 (5.3)  $\text{cm}^{-1}$  (km/mole) {degeneracy}. The bond lengths calculated in this clusters are Fe-Fe = 229.2 pm, Fe-B = 200.1 pm and Fe-Co = 235.0 pm. The vibrational spectra are shown in Appendix B.

Another design for  $\text{FeCoB}_4$  is like a shape of a building. The iron atom is on top of the pyramid, where the pyramid is formed of four boron atoms and a cobalt atom. The bond length of B-B is 162.2 pm, B-Co is 207.1 pm and Co-Fe is 218.5 pm. A strong peak appears at 780.0  $\text{cm}^{-1}$  with intensity of 69.3 km/mole and degeneracy of 2.

Table 6.2.2.1. Pictures and bond lengths of clusters  $\text{FeCo}_2\text{B}_3$  and  $\text{CoFe}_2\text{B}_3$  calculated using DFT simulations.

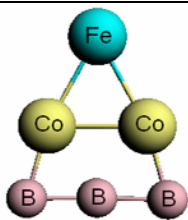
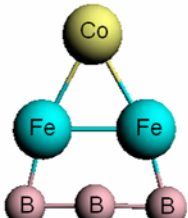
Cluster	Structure	Bond lengths (pm)
$\text{FeCo}_2\text{B}_3$		Fe-Co = 237.9 Co-Co = 224.7 Co-B = 175.4 B-B = 159.8
$\text{CoFe}_2\text{B}_3$		Co-Fe = 236.5 Fe-Fe = 230.2 Fe-B = 175.5 B-B = 159.5

Table 6.2.2.1 shows the structure of clusters  $\text{FeCo}_2\text{B}_3$  and  $\text{CoFe}_2\text{B}_3$ . As the structure becomes complicated, more vibrational frequencies are obtained. The frequencies of  $\text{FeCo}_2\text{B}_3$  are -89.6 (-1.9), 69.4 (3.8), 223.6 (3.2), 229.1 (0.8), 275.9 (1.2), 276.4 (0.003), 497.0 (0.3), 619.2 (0.8), 653.8 (0.5), 775.3 (7.97) and 1188.1 (3.5),  $\text{cm}^{-1}$  (intensities, km/mole).

The cluster  $\text{CoFe}_2\text{B}_3$  shows vibrations at -93.7  $\text{cm}^{-1}$  (-7.6 km/mole), 117.4  $\text{cm}^{-1}$  (12.6 km/mole), 220.9  $\text{cm}^{-1}$  (0.5 km/mole), 259.2  $\text{cm}^{-1}$  (1.0 km/mole), 261.5  $\text{cm}^{-1}$  (0.3 km/mole), 271.6  $\text{cm}^{-1}$  (0.7 km/mole), 491.6  $\text{cm}^{-1}$  (0.3 km/mole), 617.3  $\text{cm}^{-1}$  (3.6

km/mole),  $649.2\text{ cm}^{-1}$  (1.2 km/mole),  $774.5\text{ cm}^{-1}$  (12.4 km/mole) and  $1166.4\text{ cm}^{-1}$  (0.2 km/mole). The negative value of a frequency indicates an imaginary frequency. The reasons of negative frequencies are obtained is discussed in Appendix A.

The configuration of  $\text{Fe}_2\text{Co}_2\text{B}_2$  is in Figure 6.2.2.1. The bond lengths are Co-Co = 206.8 pm, B-B = 166.6 pm, Fe=Fe = 213.1 pm, Co-B = 186.8 pm and B-Fe = 193.9 pm. The vibrations mode are at  $-198.4\text{ cm}^{-1}$ ,  $104.8\text{ cm}^{-1}$ ,  $232.0\text{ cm}^{-1}$ ,  $235.2\text{ cm}^{-1}$ ,  $313.0\text{ cm}^{-1}$ ,  $347.6\text{ cm}^{-1}$ ,  $552.3\text{ cm}^{-1}$ ,  $699.7\text{ cm}^{-1}$  and  $844.5\text{ cm}^{-1}$  with intensities of -0.57 km/mole, 34.5 km/mole, 5.6 km/mole, 0.1 km/mole, 22.2 km/mole, 4.4 km/mole, 14.0 km/mole, 12.8 km/mole and 8.3 km/mole respectively.

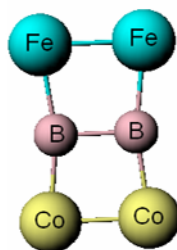


Figure 6.2.2.1. Picture of the cluster  $\text{Fe}_2\text{Co}_2\text{B}_2$ .

$\text{Fe}_2\text{Co}_3\text{B}$ , three cobalt atoms and two iron atoms formed a triangular base bipyramidal and a boron atom is on top of it. The distance among Co-Co atoms is 252.6 pm, Co-Fe atoms is 219.4 pm and Fe-B is 175.8 pm. The frequencies (intensities) {degeneracy} values are  $-86.6$  (-3.5) {2},  $114.0$  (0.5) {2},  $144.5$  (0.2),  $224.5$  (0.5) {2},  $296.5$  (9.3) {2},  $299.2$  (2.7),  $361.4$  (3.7) and  $693.9$  (1.3)  $\text{cm}^{-1}$  (km/mole).

### 6.2.3 Model 3

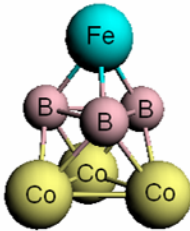
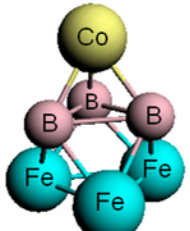
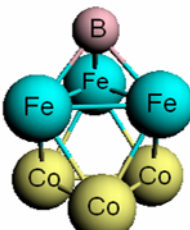
This part contains clusters of seven atoms.  $\text{FeCo}_2\text{B}_4$ ,  $\text{FeCo}_4\text{B}_2$ ,  $\text{Fe}_2\text{CoB}_4$ ,  $\text{Fe}_2\text{Co}_4\text{B}$  and  $\text{Fe}_4\text{Co}_2\text{B}$  formed the same structure where four identical atoms are in a square shape in the middle and two other atoms of the same are on each side to form a bipyramidal with

the only atom on top of the whole. The structure of  $\text{Fe}_4\text{CoB}_2$  is a bit different but the shape is the same as those of clusters above.

- i.  $\text{FeCo}_2\text{B}_4$ . The bond lengths are B-B = 176.3 pm, both sides of B-Co are equivalent where B-Co = 205.7 pm and Fe-Co = 211.8 pm. The frequencies,  $\text{cm}^{-1}$  (intensities, km/mole) {degeneracy} are -94.7 (-2.9) {2}, 177.4 (2.2), 201.3 (1.3) {2}, 327.5 (31.4), 455.8 (110.0), 468.1 (3.6) {2}, 575.9 (45.2) {2} and 801.9 (5.5).
- ii.  $\text{FeCo}_4\text{B}_2$ . The bond lengths are Co-Co = 237.3 pm, B-Co = 190.2 pm with Fe attached on top of B = 183.1 pm and the other side of B-Co = 192.0 pm. The frequencies (intensities) {degeneracy} are -129.1 (-0.04) {2}, 156.5 (0.3), 165.0 (0.0004) {2}, 315.1 (7.4), 498.9 (1.1) {2}, 560.4 (28.2) {2}, 598.5 (20.3) and 879.2 (1.3)  $\text{cm}^{-1}$  (km/mole).
- iii.  $\text{Fe}_2\text{CoB}_4$ . The bond lengths: B-B = 163.4 pm, B-Fe = 206.4 pm with a cobalt atom attached on top of Fe = 211.9 pm and the other side of B-Fe = 197.7 pm. The frequencies,  $\text{cm}^{-1}$  (intensities, km/mole): 186.4 (0.004), 207.4 (0.6), 219.7 (0.1), 219.9 (0.1), 327.7 (25.1), 408.0 (1.3), 408.2 (1.3), 452.2 (0.001), 546.9 (25.2), 866.7 (9.3), 869.8 (9.3), 887.0 (0.03) and 953.3 (7.5).
- iv.  $\text{Fe}_2\text{Co}_4\text{B}$ . The bond lengths are Co-Co = 235.0 pm, Co-Fe = 227.4 pm with a boron atom attached on top of iron atom giving length of 165.5 pm and the distance of Co-Fe on the other side is 226.0 pm. The frequencies,  $\text{cm}^{-1}$  (intensities, km/mole) {degeneracy} are 92.9 (0.003) {2}, 97.9 (0.001) {2}, 170.7 (0.02), 277.7 (5.3), 288.5 (8.8) {2}, 359.8 (8.0) and 867.9 (2.4).
- v.  $\text{Fe}_4\text{Co}_2\text{B}$ . Distance among Fe-Fe bond is 232.3 pm, Fe-Co is 230.2 pm with B on top Fe of length 166.2 pm and Fe-Co on other side with 224.6 pm. The strongest frequency is at 305.3  $\text{cm}^{-1}$  (11.8 km/mole) {2}.

- vi.  $\text{Fe}_4\text{CoB}_2$ . This cluster contains four Fe atoms as a square with a Co atom and B atom at each sides forming bipyramidal. The left B atom is on top of the whole. The bond lengths are Fe-Fe = 231.9 pm, Fe-B = 201.1 pm, Fe-Co = 229.2 pm and B-B = 165.1 pm. The largest frequency appears at  $462.1\text{ cm}^{-1}$  with intensity of 21.8 km/mole and degeneracy of two.

Table 6.2.3.1. Comparisons between clusters  $\text{FeCo}_3\text{B}_3$ ,  $\text{Fe}_3\text{CoB}_3$  and  $\text{Fe}_3\text{Co}_3\text{B}$ .

Cluster	Structure	Bond length (pm)	Strong peaks, $\text{cm}^{-1}$ (Intensity, km/mole)
$\text{FeCo}_3\text{B}_3$		Fe-B = 181.2 B-B = 190.7 B-Co = 192.0 Co-Co = 233.2	403.0 (28.2) 848.6 (39.3)
$\text{Fe}_3\text{CoB}_3$		Co-B = 184.9 B-B = 191.8 B-Fe = 189.7 Fe-Fe = 232.5	420.6 (42.0) 837.8 (38.8)
$\text{Fe}_3\text{Co}_3\text{B}$		B-Fe = 191.5 Fe-Fe = 233.3 Fe-Co = 228.6 Co-Co = 226.0	387.7 (72.5)

The clusters shown in Table 6.2.3.1 as above are quite unique where the top part of the structure is a triangular base pyramid and the three atoms at the bottom part in a triangle shape are twisted  $60^\circ$  clockwise to the base. While for clusters in Table 6.2.3.2, the structure is long where two similar atoms are at the side of a bipyramid.

Table 6.2.3.2. The comparison between clusters  $\text{Fe}_2\text{Co}_2\text{B}_3$  and  $\text{Fe}_3\text{Co}_2\text{B}_2$ .

Cluster	Structure	Bond length (pm)	Strong peaks, $\text{cm}^{-1}$ (Intensity, $\text{km/mole}$ )
$\text{Fe}_2\text{Co}_2\text{B}_3$		B-B = 165.2 B-Co = 199.1 Co-Fe = 215.6	262.7 (73.8) 460.2 (31.3)
$\text{Fe}_3\text{Co}_2\text{B}_2$		Fe-Fe = 229.0 Fe-Co = 234.2 Co-B = 165.5	62.5 (8.9) 253.6 (15.5)

#### 6.2.4 Model 4

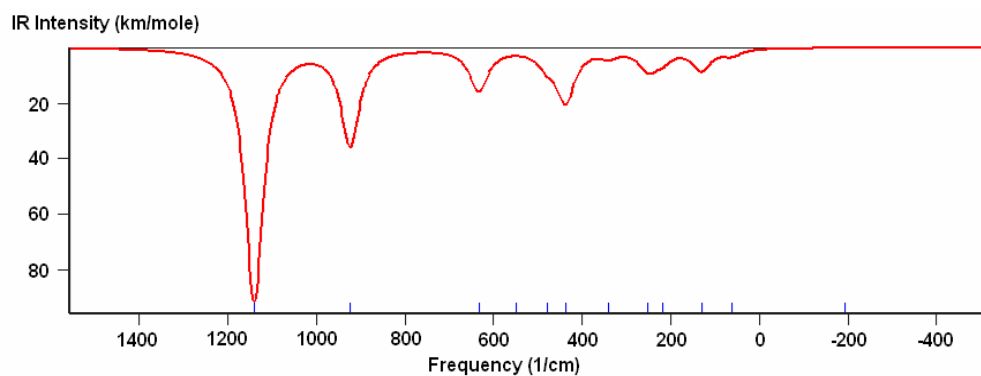
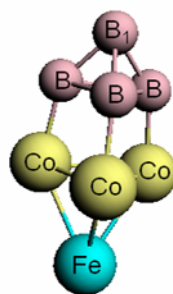


Figure 6.2.4.1. Picture and the vibrational spectrum of cluster  $\text{FeCo}_3\text{B}_4$ .



The model 4 consists of clusters with eight atoms. The clusters of  $\text{FeCo}_3\text{B}_4$ ,  $\text{Fe}_3\text{CoB}_4$ ,  $\text{Fe}_3\text{Co}_3\text{B}_2$ ,  $\text{Fe}_3\text{Co}_4\text{B}$  and  $\text{Fe}_4\text{Co}_3\text{B}$  having a crystal structure. Figure 6.2.4.1 shows picture of cluster  $\text{FeCo}_3\text{B}_4$  and the spectrum calculated using spin polarized double zeta wave functions. The bond lengths are B-B = 182.96 pm, Co-Co = 228.6 pm, Fe-Co = 239.9 pm, Co-B = 183.2 pm and B<sub>1</sub>-B = 158.3 pm. The largest frequency is the strongest peak with  $1140.4 \text{ cm}^{-1}$  (90.9 km/mole) and the other weak peaks having values at frequencies,  $\text{cm}^{-1}$  (intensities, km/mole) {degeneracy}: 62.8 (1.2) {2}, 130.6 (3.9) {2}, 219.5 (3.8), 250.9 (3.5) {2}, 339.8 (2.4), 437.6 (9.3), {2}, 479.3 (2.3) {2}, 249.1 (0.1), 633.5 (15.0) and 923.8 (17.3) {2}.

For cluster  $\text{Fe}_3\text{CoB}_4$ , the largest frequency is also the strongest peak at  $1170.4 \text{ cm}^{-1}$  (66.2 km/mole). The other peaks remaining are at frequencies,  $\text{cm}^{-1}$  (intensities, km/mole) {degeneracy}: 93.0 (0.01) {2}, 200.4 (9.04) {2}, 247.2 (0.7), 398.1 (5.6) {2}, 409.1 (8.1), 485.2 (1.2) {2}, 529.1 (0.2), 669.7 (8.4) and 874.6 (19.0) {2}.

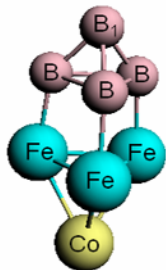
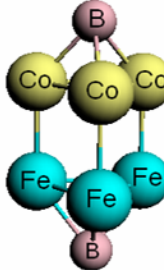
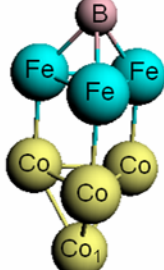
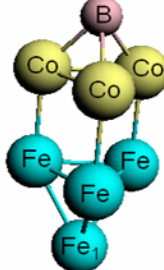
The vibrational mode for the cluster  $\text{Fe}_3\text{Co}_3\text{B}_2$  are  $89.9 \text{ cm}^{-1}$ ,  $92.9 \text{ cm}^{-1}$ ,  $220.4 \text{ cm}^{-1}$ ,  $227.8 \text{ cm}^{-1}$ ,  $238.2 \text{ cm}^{-1}$ ,  $254.8 \text{ cm}^{-1}$ ,  $306.8 \text{ cm}^{-1}$ ,  $313.6 \text{ cm}^{-1}$ ,  $337.8 \text{ cm}^{-1}$ ,  $398.5 \text{ cm}^{-1}$ ,  $659.5 \text{ cm}^{-1}$  and  $669.6 \text{ cm}^{-1}$  with intensities {degeneracy} of 0.00002 km/mole, 0.0003 km/mole {2}, 4.2 km/mole {2}, 0.4 km/mole {2}, 12.3 km/mole {2}, 0.24 km/mole, 0.003 km/mole, 31.8 km/mole, 0.3 km/mole, 2.5 km/mole {2}, 6.5 km/mole and 1.4 km/mole respectively.

The cluster  $\text{Fe}_3\text{Co}_4\text{B}$  having frequencies (intensities) {degeneracy} values at 87.4 (0.0001) {2}, 95.6 (0.00002), 134.1 (2.2) {2}, 184.9 (3.6) {2}, 212.7 (1.4), 229.7 (8.2) {2}, 243.9 (1.5) {2}, 286.7 (3.6), 308.4 (10.6) {2}, 343.4 (3.9), 374.6 (6.9) and 654.3 (0.7)  $\text{cm}^{-1}$  (km/mole).

The cluster  $\text{Fe}_4\text{Co}_3\text{B}$  shows frequencies at  $28.1 \text{ cm}^{-1}$ ,  $116.3 \text{ cm}^{-1}$ ,  $181.5 \text{ cm}^{-1}$ ,  $188.8 \text{ cm}^{-1}$ ,  $224.6 \text{ cm}^{-1}$ ,  $240.6 \text{ cm}^{-1}$ ,  $258.1 \text{ cm}^{-1}$ ,  $299.4 \text{ cm}^{-1}$ ,  $360.7 \text{ cm}^{-1}$ ,  $368.5 \text{ cm}^{-1}$  and  $654.4 \text{ cm}^{-1}$  with intensities {degeneracy} of 0.00002 km/mole, 4.7 km/mole {2}, 0.36

km/mole, 2.8 km/mole {2}, 2.7 km/mole {2}, 0.08 km/mole {2}, 2.9 km/mole, 0.2 km/mole, 21.4 km/mole, 3.3 km/mole {2} and 2.9 km/mole respectively. The bond lengths of cluster  $\text{Fe}_3\text{CoB}_4$ ,  $\text{Fe}_3\text{Co}_3\text{B}_2$ ,  $\text{Fe}_3\text{Co}_4\text{B}$  and  $\text{Fe}_4\text{Co}_3\text{B}$  are list in Table 6.2.4.1 as below.

Table 6.2.4.1. Bond lengths for cluster  $\text{Fe}_3\text{CoB}_4$ ,  $\text{Fe}_3\text{Co}_3\text{B}_2$ ,  $\text{Fe}_3\text{Co}_4\text{B}$  and  $\text{Fe}_4\text{Co}_3\text{B}$ .

$\text{Fe}_3\text{CoB}_4$	$\text{Fe}_3\text{Co}_3\text{B}_2$	$\text{Fe}_3\text{Co}_4\text{B}$	$\text{Fe}_4\text{Co}_3\text{B}$
			
Bond lengths (pm)	Bond lengths (pm)	Bond lengths (pm)	Bond lengths (pm)
$\text{B}_1\text{-B} = 157.9$	$\text{B-Co} = 190.1$	$\text{B-Fe} = 195.3$	$\text{B-Co} = 190.6$
$\text{B-B} = 181.5$	$\text{Co-Co} = 229.0$	$\text{Fe-Fe} = 224.4$	$\text{Co-Co} = 225.5$
$\text{B-Fe} = 190.2$	$\text{Co-Fe} = 226.2$	$\text{Fe-Co} = 223.1$	$\text{Co-Fe} = 235.6$
$\text{Fe-Fe} = 218.4$	$\text{Fe-Fe} = 227.1$	$\text{Co-Co} = 227.0$	$\text{Fe-Fe} = 227.4$
$\text{Fe-Co} = 233.6$	$\text{Fe-B} = 194.5$	$\text{Co}_1\text{-Co} = 227.6$	$\text{Fe-Fe}_1 = 234.7$

### 6.2.5 Model 5

The clusters of nine atoms formed are grouped as model 5. Degenerate states can be found for each of the clusters as different possible occupation states for the clusters may be related by symmetry. In this chapter there are some clusters which are in symmetry shapes. Structures and bond lengths in  $\text{FeCo}_4\text{B}_4$  and  $\text{Fe}_4\text{CoB}_4$  are shown in table 6.2.5.1.

The vibrational frequencies for cluster  $\text{FeCo}_4\text{B}_4$  are  $208.8 \text{ cm}^{-1}$ ,  $246.5 \text{ cm}^{-1}$ ,  $265.1 \text{ cm}^{-1}$ ,  $335.5 \text{ cm}^{-1}$ ,  $572.3 \text{ cm}^{-1}$ ,  $644.3 \text{ cm}^{-1}$ ,  $745.3 \text{ cm}^{-1}$  and  $904.8 \text{ cm}^{-1}$  with intensities {degeneracy} of 0.07 km/mole {2}, 2.6 km/mole {2}, 7.4 km/mole, 4.1 km/mole, 0.7 km/mole {2}, 37.0 km/mole, 35.8 km/mole {2} and 13.0 km/mole respectively.

Cluster  $\text{Fe}_4\text{CoB}_4$  having frequencies (intensities) {degeneracy} values at -184.3 (-6.8) {2}, 167.3 (2.8) {2}, 211.4 (4.8), 307.0 (8.7) {2}, 359.5 (0.6), 395.5 (50.1) {2}, 477.1 (11.6), 836.9 (15.9) {2} and 914.9 (2.5)  $\text{cm}^{-1}$  (km/mole).

Table 6.2.5.1. Cluster  $\text{FeCo}_4\text{B}_4$  and  $\text{Fe}_4\text{CoB}_4$  with their respective bond lengths.

Cluster	Structure	Bond lengths (pm)
$\text{FeCo}_4\text{B}_4$		Fe-B = 190.9 B-B = 176.4 B-Co = 179.9 Co-Co = 224.5
$\text{Fe}_4\text{CoB}_4$		Co-Fe = 236.4 Fe-Fe = 215.7 Fe-B = 198.4 B-B = 162.7

Clusters of  $\text{FeCo}_4\text{B}_4$  having a crown shape where the top part of the structure is made up of four cobalt atoms and an iron atom as a square base pyramid and the other four boron atoms left are at the bottom part in a square shape which is twisted  $45^\circ$  clockwise to the pyramid's base. The bond lengths formed are Fe-Co = 227.4 pm, Co-Co = 261.3 pm, Co-B = 191.9 pm and B-B = 166.4 pm. The vibration modes (intensities) {degeneracy} are 122.2 (2.0) {2}, 171.2 (0.8), 247.0 (15.3) {2}, 298.8 (3.8), 349.1 (0.8) {2}, 444.8 (0.001), 503.3 (56.7) {2}, 577.6 (1.2), 848.9 (0.06) and 859.6 (4.1) {2}  $\text{cm}^{-1}$  (km/mole).

$\text{Fe}_3\text{Co}_3\text{B}_3$ , forms a shape where three layers of triangle are stacked on top of each other. The cobalt layer is in the middle of the boron layer and iron layer. The distance between B-B bond is 163.0 pm, Co-Co bond is 233.6 pm, Fe-Fe bond is 215.7 pm, B-Co bond is 188.2 pm and Co-Fe bond is 231.6 pm. The frequencies (intensities)

{degeneracy} are 58.2 (0.00001), 161.9 (3.5) {2}, 203.8 (4.6) {2}, 214.1 (0.4), 230.2 (5.1) {2}, 278.4 (0.3), 366.3 (16.9), 442.6 (0.1) {2}, 530.0 (3.7), 698.9 (3.4) {2} and 1002.2 (3.9)  $\text{cm}^{-1}$  (km/mole).

## 6.2.6 Model 6

There are two types of structures that are built with total number atoms of 10.  $\text{Fe}_4\text{Co}_4\text{B}_2$ ,  $\text{Fe}_4\text{Co}_2\text{B}_4$  are having structures of the same kind where two bipyramids are combined together in a symmetric way. The bond lengths in cluster  $\text{Fe}_4\text{Co}_4\text{B}_2$  are B-Co = 194.4 pm, Co-Co = 223.5 pm, Co-Fe = 228.9 pm, Fe-Fe = 226.4 pm and Fe-B = 200.8 pm. The strongest peak appears to be at  $330.7 \text{ cm}^{-1}$  with intensity of 42.4 km/mole and degeneracy 2. The other peaks remaining are  $-90.7$  (-0.003) {2}, 195.4 (3.1) {2}, 226.0 (6.6) {2}, 240.7 (4.7) {2}, 243.6 (0.001), 269.1 (1.8), 287.3 (4.9), 482.0 (9.4) {2}, 581.1 (0.8) and  $595.7$  (1.1)  $\text{cm}^{-1}$  (km/mole).

The bond lengths in cluster  $\text{Fe}_4\text{Co}_2\text{B}_4$  are Co-Fe = 226.2 pm, Fe-Fe = 235.4 pm, Fe-B = 188.2 pm, B-B = 177.6 pm and B-Co = 189.8 pm. The frequencies (intensities) {degeneracy} are  $-202.5$  (-0.9) {2}, 150.3 (0.06) {2}, 192.7 (0.003), 225.0 (0.01) {2}, 288.2 (8.8) {2}, 289.3 (6.9), 346.8 (11.1), 524.9 (4.1) {2}, 555.9 (59.50), 703.0 (19.2) {2} and  $902.6$  (15.5)  $\text{cm}^{-1}$  (km/mole).

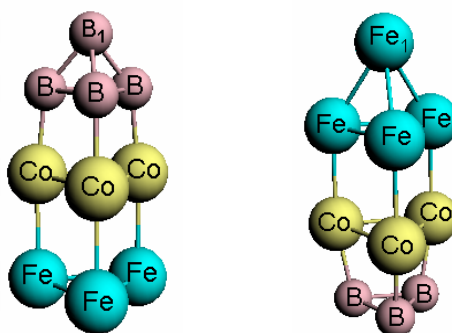


Figure 6.2.6.1. Structure of cluster  $\text{Fe}_3\text{Co}_3\text{B}_4$  and cluster  $\text{Fe}_4\text{Co}_3\text{B}_3$ .

The bond lengths in cluster  $\text{Fe}_3\text{Co}_3\text{B}_4$  shown in Figure 6.2.6.1 are B<sub>1</sub>-B = 158.4 pm, B-B = 181.5 pm, B-Co = 185.2 pm, Co-Co = 223.4 pm, Co-Fe = 233.6 pm and Fe-Fe = 221.7 pm. While the bond lengths for  $\text{Fe}_4\text{Co}_3\text{B}_3$  on the right side of the figure are Fe<sub>1</sub>-Fe = 235.8 pm, Fe-Fe = 230.0 pm, Fe-Co = 237.9 pm, Co-Co = 230.1 pm, Co-B = 186.9 pm and B-B = 162.5 pm.

The largest frequency value for  $\text{Fe}_3\text{Co}_3\text{B}_4$  is  $1157.7 \text{ cm}^{-1}$  with intensity 134.9 km/mole and the weak peaks having frequencies (intensities) {degeneracy} at -108.2 (-0.2) {2}, -71.8 (-0.02) {2}, 193.9 (0.02), 194.0 (3.4) {2}, 213.6 (4.7) {2}, 241.3 (1.1) {2}, 338.1 (0.3), 357.3 (17.6), 412.2 (0.8) {2}, 471.9 (0.05) {2}, 517.6 (19.0), 644.2 (14.4) and  $900.9 (3.5) \text{ cm}^{-1}$  (km/mole). While cluster  $\text{Fe}_4\text{Co}_3\text{B}_3$  having the largest value at  $353.6 \text{ cm}^{-1}$  with intensity (21.1 km/mole) and the remaining frequencies,  $\text{cm}^{-1}$  (intensities, km/mole) {degeneracy} are -249.9 (-2.9) {2}, -195.2 (-0.3), -78.6 (-1.3) {2}, -46.7 (-0.0009), 123.9 (1.7) {2}, 164.0 (1.3) {2}, 171.9 (1.3), 198.4 (4.1) {2}, 239.8 (2.4) {2}, 244.9 (5.6), 305.9 (0.1), 493.7 (0.7) {2}, 546.9 (0.4), 719.7 (3.8) {2} and 1015.0 (0.25).

## 6.2.7 Model 7

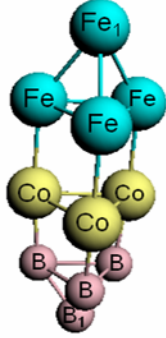
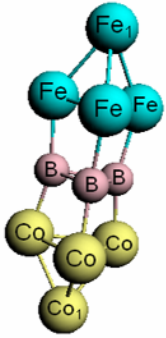
Table 6.2.7.1 illustrates the comparisons between clusters  $\text{Fe}_4\text{Co}_3\text{B}_4$  and  $\text{Fe}_4\text{Co}_4\text{B}_3$  in terms of structures and bond lengths. In this part, these two clusters contain 11 atoms.

For cluster  $\text{Fe}_4\text{Co}_3\text{B}_4$ , the largest frequency is the strongest peak at  $1147.7 \text{ cm}^{-1}$  with intensity 100.97 km/mole. The remaining frequencies (intensities) {degeneracy} are at -117.5 (-2.8) {2}, -88.3 (-0.003) {2}, 108.6 (0.9) {2}, 164.9 (3.8), 177.7 (5.2) {2}, 182.7 (1.7) {2}, 232.6 (0.96) {2}, 239.1 (9.6), 313.8 (2.9), 343.3 (14.6), 416.3 (0.3) {2}, 469.9 (0.3) {2}, 521.1 (10.5), 653.6 (17.1) and  $887.3 (14.1) \text{ cm}^{-1}$  (km/mole).

The cluster  $\text{Fe}_4\text{Co}_4\text{B}_3$  having frequencies,  $\text{cm}^{-1}$  (intensities, km/mole) {degeneracy} values at -189.8 (-32.7) {2}, -153.9 (-1.6) {2}, 86.3 (2.7) {2}, 90.8 (1.0)

{2}, 162.9 (0.6), 164.5 (0.4) {2}, 203.9 (6.7) {2}, 223.7 (11.3) {2}, 236.9 (4.1), 268.7 (0.4), 342.8 (23.8), 360.6 (10.6), 551.8 (0.3) {2}, 597.0 (6.4) {2}, 675.1 (27.6) and 841.0 (1.2).

Table 6.2.7.1. Comparisons between clusters  $\text{Fe}_4\text{Co}_3\text{B}_4$  and  $\text{Fe}_4\text{Co}_4\text{B}_3$ .

Cluster	Structure	Bond lengths (pm)
$\text{Fe}_4\text{Co}_3\text{B}_4$		$\text{Fe}_1\text{-Fe} = 234.8$ $\text{Fe-Fe} = 231.5$ $\text{Fe-Co} = 237.6$ $\text{Co-B} = 184.6$ $\text{Co-Co} = 225.6$ $\text{B-B} = 181.0$ $\text{B-B}_1 = 158.5$
$\text{Fe}_4\text{Co}_4\text{B}_3$		$\text{Fe}_1\text{-Fe} = 238.8$ $\text{Fe-Fe} = 225.5$ $\text{Fe-B} = 200.3$ $\text{B-B} = 170.8$ $\text{B-Co} = 187.3$ $\text{Co-Co} = 231.7$ $\text{Co-Co}_1 = 228.2$

### 6.3 Analysis

The vibrational frequencies of the clusters are found to be dependent on the local environment and on the structure. When there are 5 atoms in a cluster, the largest frequency is  $933 \text{ cm}^{-1}$ . In this system, three B atoms are connected to Fe atoms and Co is on top of the Fe atom. The largest frequency indicates the largest force constant. When six atoms are present, the largest frequency occurred in a configuration in which three B atoms are located in the bottom with two Co atoms in the next line above that of B and one Fe is on top. In this configuration of six atoms, the largest frequency is found to be  $1188 \text{ cm}^{-1}$ . Amongst the clusters containing seven atoms, the largest value of  $953.3 \text{ cm}^{-1}$  is found for  $\text{Fe}_2\text{CoB}_4$ . Whereas, among the clusters which containing

eight atoms,  $\text{Fe}_3\text{CoB}_4$ , has the largest frequency of  $1170.4 \text{ cm}^{-1}$ . Next,  $\text{Fe}_3\text{Co}_3\text{B}_3$  has the largest frequency of  $1002.2 \text{ cm}^{-1}$ ,  $\text{Fe}_3\text{Co}_3\text{B}_4$  has the largest frequency of  $1157.4 \text{ cm}^{-1}$  and  $\text{B}_4\text{Co}_3\text{Fe}_4$  has the largest frequency of  $1147.7 \text{ cm}^{-1}$  for clusters containing 9, 10 and 11 atoms respectively. Thus, by changing the composition of the atoms, the force constant of the material can be changed.

## 6.4 Conclusions

By very extensive calculation of vibrational frequencies of clusters of atoms, the composition and force constants are found to be adjustable. Ability of the electrons to be spin-polarized [37] on the ferromagnetic materials can be found. In this way, the composition suited for the memory material can be predicted.

# CHAPTER 7

## Conclusions

The first three chapters review the need for a magnetoresistance random access memory (MRAM) material and the density-functional theory used to solve the problem of the calculation of vibrational frequencies of a very large secular determinant in quantum mechanics. In chapter 4, the largest frequency of each group of the cluster  $\text{NiFe}_n$ ,  $\text{Ni}_2\text{Fe}_n$ ,  $\text{Ni}_3\text{Fe}_n$  and  $\text{Ni}_4\text{Fe}_n$  as function of concentration is calculated and described in detail. The overall trend of clusters  $\text{NiFe}_n$  shows a positive gradient although there is a plateau between  $n=2$  and 3. The largest value is at  $n=4$  with frequency of  $377.3 \text{ cm}^{-1}$ . The  $\text{Ni}_2\text{Fe}_n$  clusters show an increment from  $n=1$  to 2 and is almost flat around  $n=3$  and 4. The turning point from the sloppiest part to the flat part is around  $n=3$  where the frequency shows at  $323.5 \text{ cm}^{-1}$ . At  $n=3$  having both the properties of the turning point and the largest phonon frequency, where this cluster may be indicating unique physical properties.  $\text{Ni}_3\text{Fe}_n$  shows that the largest frequency reduces as a function of  $n$  in a parabola shape. The minimum value is at  $n=2$ . While for cluster group  $\text{Ni}_4\text{Fe}_n$ , the trend is almost the same as in  $\text{Ni}_4\text{Fe}_n$ .

The four groups above are summarized, they are identical at  $n=4$  where the value goes up to a maximum.  $\text{NiFe}_n$  and  $\text{Ni}_2\text{Fe}_n$  shows low value at  $n=1$  but shoot up at  $n=4$  whereas  $\text{Ni}_3\text{Fe}_n$  and  $\text{Ni}_4\text{Fe}_n$  show minimum around  $n=2$  and 3 and goes up at  $n=4$ . As nickel increases with the number, the function of  $\text{NiFe}_n$  and  $\text{Ni}_2\text{Fe}_n$  is almost equivalent as well as  $\text{Ni}_3\text{Fe}_n$  with  $\text{Ni}_4\text{Fe}_n$ . But as the number of iron increases for each



group, the value of the frequency increases. Thus, the magnetization of the cluster increases. The higher magnetization in the ferromagnetic layers is important for shorter read time access.

The small clusters of  $\text{Fe}_x\text{Co}_y\text{B}_z$  consist of 3 and 4 atoms as described in chapter 5. For 3 atoms, cluster Fe-Co-B appears to be having the largest frequency and also the strongest peak,  $912.3 \text{ cm}^{-1}$  with intensity 17.7 km/mole.

When the total number of atoms increases to 4, the cluster with the largest vibrational frequency,  $880.4 \text{ cm}^{-1}$  is  $\text{CoBFe}_2$  in a triangular structure. When the configuration is changed to  $\text{BFeCo}_2$  yet in the same structure, it gives a frequency value at  $502.6 \text{ cm}^{-1}$  (0.32 km/mole), which is the smallest value among all of the clusters for total of 4 atoms. Comparing  $\text{CoBFe}_2$  with  $\text{BFeCo}_2$ , it is found that the atomic configuration of a material is important in determining the phonon frequency which gives the force constants.

Since phonon frequencies are correlated with the resistance between the ferromagnetic layers, it is essential knowing the frequencies of the clusters in forming the best MRAM materials. Linear Fe-Co-B shows the largest vibrational frequency and thus, having the strongest force constant for clusters of a total of 3 atoms.

Chapter 6 is the continuous part of chapter 5 which contains of cluster of total of 5 atoms.  $\text{FeCoB}_3$  (enlongated triangle-based pyramid) and  $\text{FeCoB}_3$  (symmetric bipyramid) gives frequency at  $933.0 \text{ cm}^{-1}$  (50.8 km/mole) and  $858.0 \text{ cm}^{-1}$  (1.7 km/mole). Although the atomic configuration is the same, but the structure arrangement affects the vibrational mode. This also happened to other clusters as  $\text{Fe}_3\text{CoB}$  (enlongated triangle based pyramid) with  $825.5 \text{ cm}^{-1}$  and  $\text{Fe}_3\text{CoB}$  (symmetric bipyramid) with  $714.0 \text{ cm}^{-1}$ . The largest phonon frequency of total 5 atoms is  $\text{FeCoB}_3$  (enlongated triangle based pyramid) with  $933.0 \text{ cm}^{-1}$ .

Referring to Appendix B, Table 6.2.2, the trend of the spectra of  $\text{FeCoB}_4$  (bipyramidal),  $\text{FeCo}_4\text{B}$  (bipyramidal),  $\text{Fe}_4\text{CoB}$  (bipyramidal) and  $\text{FeCoB}_4$  are almost the same with a strong peak in the middle. This shows that these four clusters have the similar same physical properties. Even though cluster  $\text{FeCoB}_4$  (bipyramid) and cluster  $\text{FeCoB}_4$  having the same configuration yet the strongest peak (large intensity) differ a little between  $737.9 \text{ cm}^{-1}$  and  $780.0 \text{ cm}^{-1}$ .  $\text{FeCo}_2\text{B}_3$  having the largest frequency value of  $1188.1 \text{ cm}^{-1}$  and  $\text{CoFeB}_3$  is the second largest with value of  $1166.4 \text{ cm}^{-1}$ . The structure with 3 boron atoms at the lower part shows large vibrational mode indicating large force constant.

The clusters with total 7 atoms,  $\text{Fe}_2\text{CoB}_4$  give the largest frequency at value  $953.3 \text{ cm}^{-1}$  ( $7.5 \text{ km/mole}$ ). In the model 3, the spectra of each cluster vary except for  $\text{FeCo}_3\text{B}_3$  and  $\text{Fe}_3\text{CoB}_3$  which seems to be alike. Comparing the clusters with total number of 5 and 6 atoms, clusters with the same number of boron atoms show spectrum which are almost identical.

Proceeding to clusters of 8 atoms, the largest frequency is at  $1170.4 \text{ cm}^{-1}$  of cluster  $\text{Fe}_3\text{CoB}_4$ . The overall function of the largest phonon frequency with respect to the number of iron atoms shows a negative gradient. This is in contrast with the situation in cluster  $\text{Fe}_x\text{Ni}_y$  where the frequency increases as a function of number of iron atoms. When the iron atoms increases, the boron atoms decreases. Since boron atoms have great effect to the cluster configuration, it is believed that the decreasing function is due to the number of boron atoms in the cluster.

As the number of atoms increases, the number of vibrational modes increases. There are more bonding pairs in the cluster and thus each bond will contribute to the vibrational mode. For cluster with 9 atoms, the largest frequency is  $\text{Fe}_3\text{Co}_3\text{B}_3$  with  $1002.2 \text{ cm}^{-1}$ .

Structure of  $\text{Fe}_3\text{Co}_3\text{B}_4$  gives the largest value at  $1157.7 \text{ cm}^{-1}$  and the second largest value,  $\text{Fe}_4\text{Co}_3\text{B}_3$  at  $1015.0 \text{ cm}^{-1}$  with shapes in stack layers. The ‘stack’ structure having group of boron atoms at the edge of both the clusters gives a high frequency value. For the last model with 11 atoms, the largest frequency with  $1147.7 \text{ cm}^{-1}$  belongs to  $\text{Fe}_4\text{Co}_3\text{B}_4$ . This cluster also has four of boron atoms at the edge whereas cluster  $\text{Fe}_4\text{Co}_4\text{B}_3$  with boron atoms in the middle of the structure only show the largest frequency at  $841.0 \text{ cm}^{-1}$ . The structures are important in the clusters for different frequencies and different force constants.

Determining the vibrational frequencies through simulation of clusters, force constant of different structure of clusters can be achieved. The composition and force constants are found to be adjustable due to different structures and configuration of clusters. The magnetization changes when nickel is added to the clusters  $\text{Fe}_x\text{Ni}_y$  as well as the boron and cobalt atoms added to clusters  $\text{Fe}_x\text{Co}_y\text{B}_z$ . The capability of electrons to be spin-polarized on the surfaces of ferromagnetic layers can be found. Therefore, through extensive calculation, better materials based on the largest frequency for the ferromagnetic layers in the cell can be predicted for higher MR in MRAM.

# List of Publications

1. Lee Li Ling, Teh Yee Lin, Hasan Abu Kassim and Keshav N. Shrivastava (2007). Stable carbon circles C14: Density-functional theory calculations, 3rd MPSGC, P2PY-1, pp. 184-188.
2. Lee Li Ling, C. Jesudason and Keshav N. Shrivastava (2009). Computerized Simulation of Magnetoresistance Random Access Memory Material, AIP Conf. Proc. 1169, pp. 279-282. **SCOPUS**
3. Lee Li Ling, Christopher Jesudason and Keshav N. Shrivastava (2009). DFT Calculation of Vibrational Frequencies of FeCoB m-RAM, AIP conference Proceedings. (Submitted).
4. Large clusters of Fe-Co-Ni atoms in RAM, Sains Malaysiana (Submitted) ISI.

## Conferences:

- (a) Computerized simulation of magnetoresistance RAM, AMNRE Jakarta (June 2009).
- (b) DFT calculation of vibrational frequencies of FeCoB MRAM, PERFIK2009 Malacca 2009.

# Appendix A

## Observation of harmonics

Usually the energy level transitions are observed according to quantization of energy as,

$$E_1 - E_2 = h\nu$$

$$\omega_1 - \omega_2 = \omega$$

For negative values,

$$\omega_1 - (-\omega_2) = \omega_0$$

$$\omega_1 + \omega_2 = \omega_0 \quad \text{This will be observed.}$$

The negative frequencies will be observed in the experiments as sum of the frequencies.

For example:  $\omega_1 = 250 \text{ cm}^{-1}$

$$\omega_2 = -100 \text{ cm}^{-1}$$

$$\omega_1 + \omega_2 = 150 \text{ cm}^{-1}$$

$$\omega_1 - (-\omega_2) = 350 \text{ cm}^{-1} \text{ will be observed.}$$

Harmonics  $\omega_1 + n\omega_2$  will be observed. The computation performance gives both positive as well as negative frequencies.

# Appendix B

Table 4.3. The vibrational spectrum for clusters  $Ni_xFe_y$  from chapter 4.

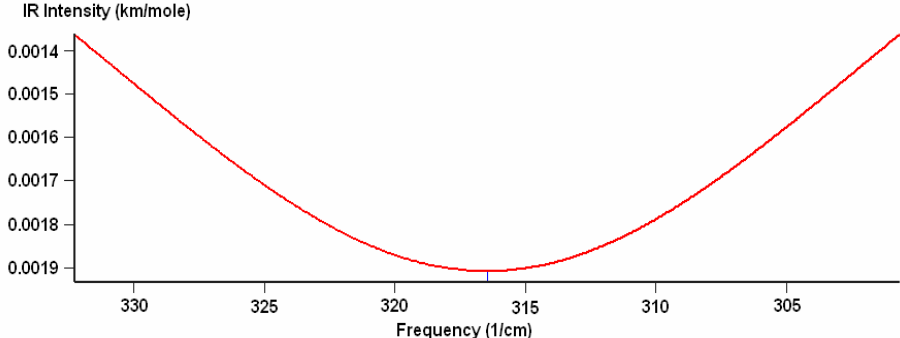
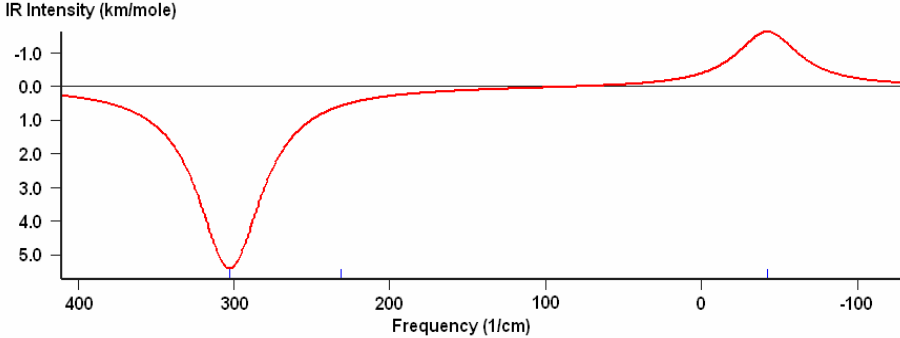
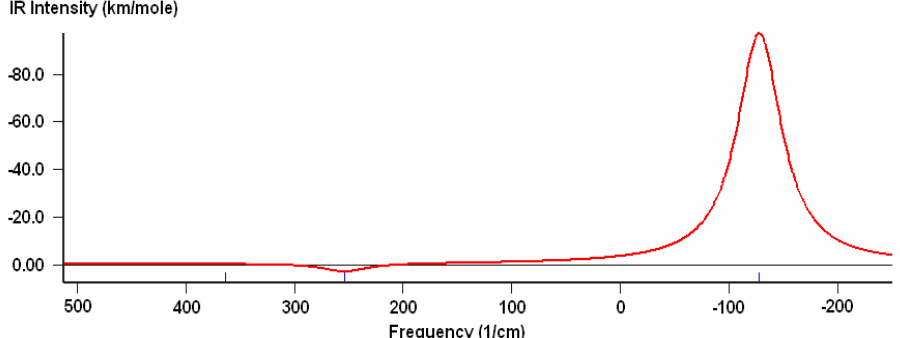
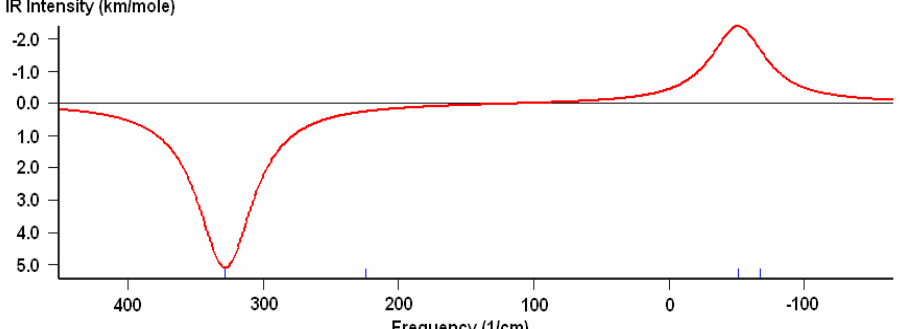
Cluster	Spectrum
NiFe	
NiFe <sub>2</sub> linear	
NiFe <sub>2</sub> triangular	
NiFe <sub>3</sub> triangular	

Table 4.3. Continued

Cluster	Spectrum
$\text{NiFe}_3$ pyramidal	<p>IR Intensity (km/mole)</p> <p>Frequency (1/cm)</p>
$\text{NiFe}_4$ square	<p>IR Intensity (km/mole)</p> <p>Frequency (1/cm)</p>
$\text{NiFe}_4$ pyramidal	<p>IR Intensity (km/mole)</p> <p>Frequency (1/cm)</p>
$\text{NiFe}_4$ tetrahedral	<p>IR Intensity (km/mole)</p> <p>Frequency (1/cm)</p>
$\text{Ni}_2\text{Fe}$ linear	<p>IR Intensity (km/mole)</p> <p>Frequency (1/cm)</p>

Table 4.3. Continued

Cluster	Spectrum
$\text{Ni}_2\text{Fe}$ triangular	
$\text{Ni}_2\text{Fe}_2$ rectangular	
$\text{Ni}_2\text{Fe}_3$ bipyramidal	
$\text{Ni}_2\text{Fe}_4$ bipyramidal	
$\text{Ni}_3\text{Fe}$ triangular	



Table 4.3. Continued

Cluster	Spectrum
$\text{Ni}_3\text{Fe}_2$ bipyramidal	
$\text{Ni}_3\text{Fe}_3$ hexagonal	
$\text{Ni}_3\text{Fe}_3$ triangle inside triangle	
$\text{Ni}_4\text{Fe}$ pyramidal	
$\text{Ni}_4\text{Fe}$ planar	

Table 4.3. Continued

Cluster	Spectrum
$\text{Ni}_4\text{Fe}_2$ bipyramidal	
$\text{Ni}_4\text{Fe}_3$ boat shape	
$\text{Ni}_4\text{Fe}_4$ deformed cube	
$\text{Ni}_4\text{Fe}_4$ square inside square	

Table 5.3. Spectrum of small clusters  $\text{Fe}_x\text{Co}_y\text{B}_z$  using double zeta spin polarized orbitals in chapter 5.

Cluster	Spectrum
FeCoB linear	
Co-Fe-B linear	
Fe-B-Co linear	
FeCoB triangular	
BFeCoB linear	

Table 5.3. Continued

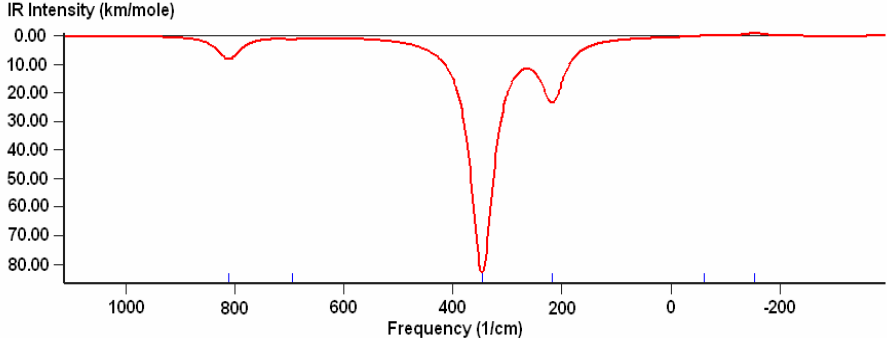
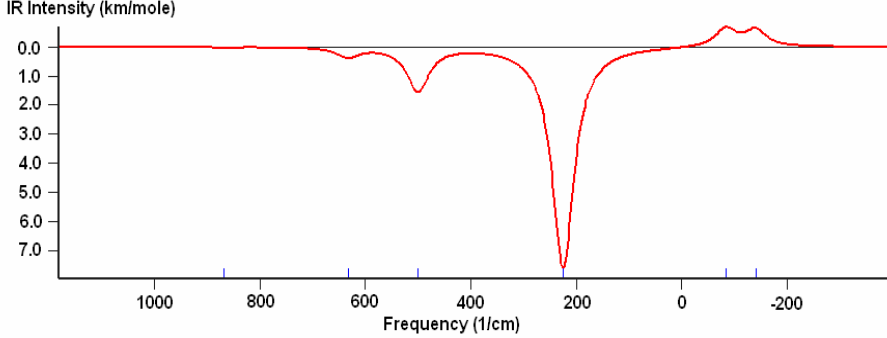
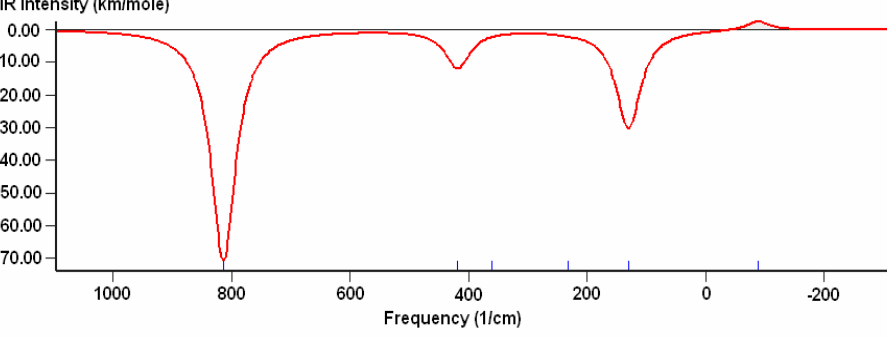
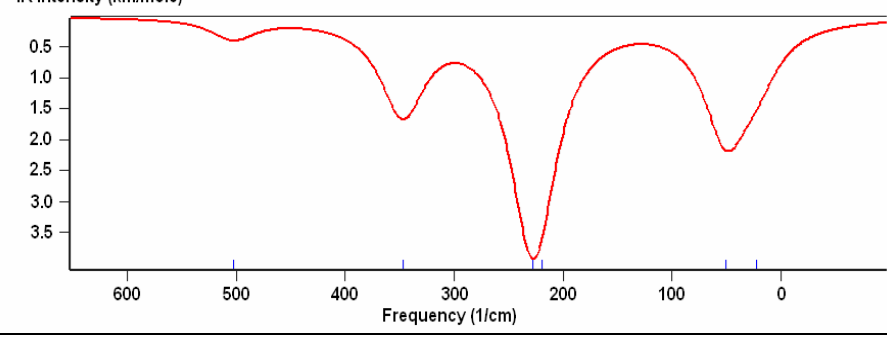
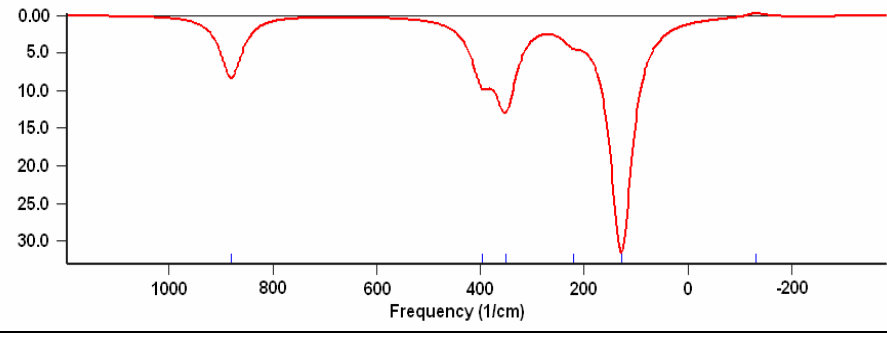
Cluster	Spectrum
CoFeB <sub>2</sub> triangular	 <p>IR Intensity (km/mole)</p> <p>Frequency (1/cm)</p> <p>The plot shows IR Intensity (km/mole) on the y-axis (0.00 to 80.00) and Frequency (1/cm) on the x-axis (1000 to -200). The spectrum features a sharp peak at approximately 350 1/cm and a broader peak at approximately 250 1/cm.</p>
FeCoB <sub>2</sub> triangular	 <p>IR Intensity (km/mole)</p> <p>Frequency (1/cm)</p> <p>The plot shows IR Intensity (km/mole) on the y-axis (0.0 to 7.0) and Frequency (1/cm) on the x-axis (1000 to -200). The spectrum features a sharp peak at approximately 250 1/cm and a broader peak at approximately 350 1/cm.</p>
FeCo <sub>2</sub> B triangular	 <p>IR Intensity (km/mole)</p> <p>Frequency (1/cm)</p> <p>The plot shows IR Intensity (km/mole) on the y-axis (0.00 to 70.00) and Frequency (1/cm) on the x-axis (1000 to -200). The spectrum features a sharp peak at approximately 800 1/cm and a broader peak at approximately 250 1/cm.</p>
BFeCo <sub>2</sub> triangular	 <p>IR Intensity (km/mole)</p> <p>Frequency (1/cm)</p> <p>The plot shows IR Intensity (km/mole) on the y-axis (0.5 to 3.5) and Frequency (1/cm) on the x-axis (600 to 0). The spectrum features a sharp peak at approximately 250 1/cm and a broader peak at approximately 350 1/cm.</p>
CoBFe <sub>2</sub> triangular	 <p>IR Intensity (km/mole)</p> <p>Frequency (1/cm)</p> <p>The plot shows IR Intensity (km/mole) on the y-axis (0.00 to 30.0) and Frequency (1/cm) on the x-axis (1000 to -200). The spectrum features a sharp peak at approximately 250 1/cm and a broader peak at approximately 350 1/cm.</p>

Table 5.3. Continued

Cluster	Spectrum
<p>B-Co-B-Fe rectangular</p>	
<p>FeCo<sub>2</sub>B rectangular</p>	
<p>Fe<sub>2</sub>CoB distorted rectangular</p>	

Table 6.2.1. Spectrum for large clusters  $\text{Fe}_x\text{Co}_y\text{B}_z$  in model 1 of chapter 6.

Cluster	Spectrum
$\text{FeCoB}_3$	<p>IR Intensity (km/mole)</p> <p>0.00 10.0 20.0 30.0 40.0 50.0</p> <p>1200 1000 800 600 400 200 0 -200</p> <p>Frequency (1/cm)</p>
$\text{Fe}_3\text{CoB}$	<p>IR Intensity (km/mole)</p> <p>0.00 5.0 10.0 15.0 20.0 25.0 30.0</p> <p>1000 800 600 400 200 0 -200</p> <p>Frequency (1/cm)</p>
$\text{FeCo}_2\text{B}_2$	<p>IR Intensity (km/mole)</p> <p>10 20 30 40 50</p> <p>800 600 400 200 0</p> <p>Frequency (1/cm)</p>
$\text{Fe}_2\text{CoB}_2$	<p>IR Intensity (km/mole)</p> <p>10 20 30 40 50 60</p> <p>900 800 700 600 500 400 300 200 100 0</p> <p>Frequency (1/cm)</p>

Table 6.2.1. Continued

Cluster	Spectrum
Fe <sub>2</sub> Co <sub>2</sub> B	
FeCoB <sub>3</sub> bipyramidal	
FeCo <sub>3</sub> B bipyramidal	
Fe <sub>3</sub> CoB bipyramidal	

Table 6.2.2. Spectrum for large clusters  $\text{Fe}_x\text{Co}_y\text{B}_z$  in model 2 of chapter 6.

Cluster	Spectrum
$\text{FeCoB}_4$ bipyramidal	<p>IR Intensity (km/mole)</p> <p>Frequency (1/cm)</p>
$\text{FeCo}_4\text{B}$ bipyramidal	<p>IR Intensity (km/mole)</p> <p>Frequency (1/cm)</p>
$\text{Fe}_4\text{CoB}$ bipyramidal	<p>IR Intensity (km/mole)</p> <p>Frequency (1/cm)</p>
$\text{FeCoB}_4$	<p>IR Intensity (km/mole)</p> <p>Frequency (1/cm)</p>



Table 6.2.2. Continued

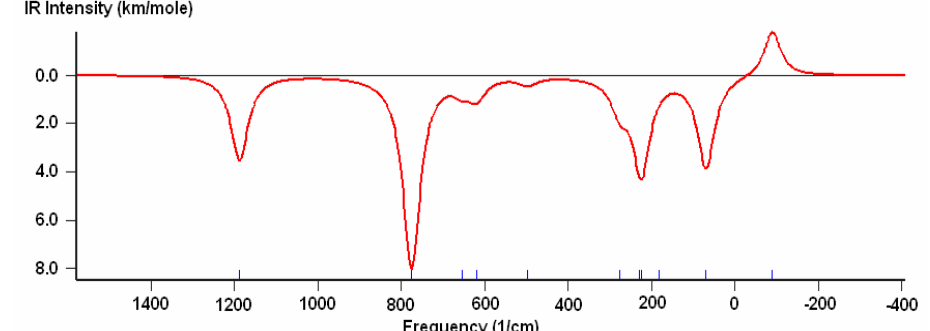
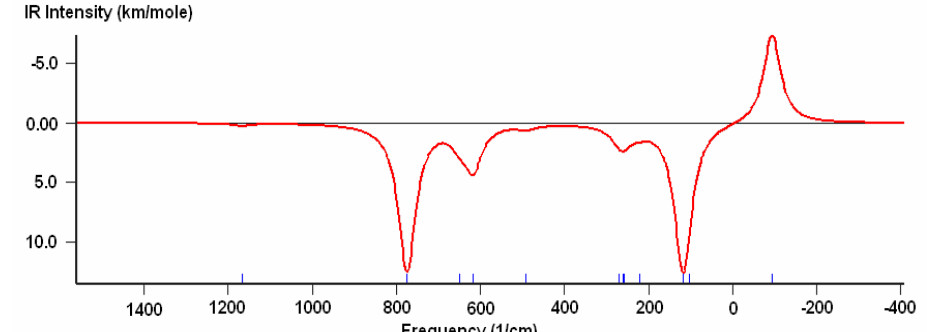
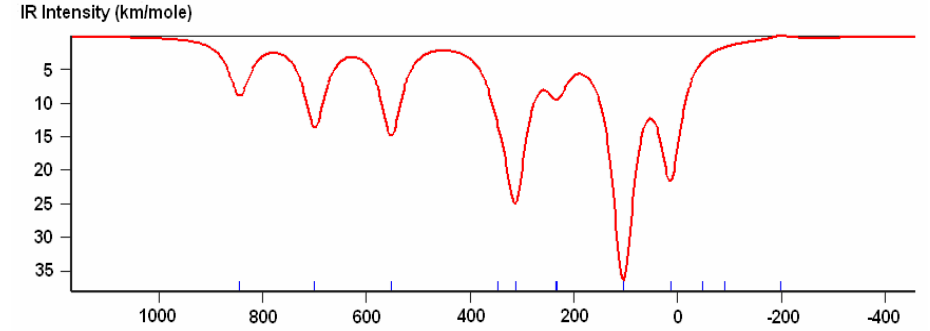
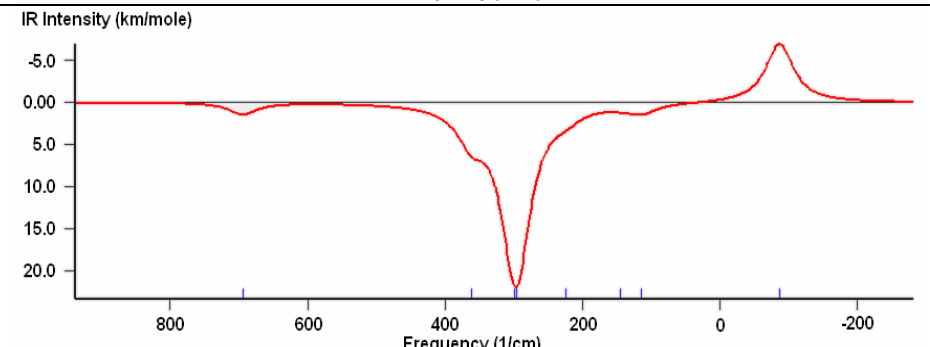
Cluster	Spectrum
FeCo <sub>2</sub> B <sub>3</sub>	 <p>IR Intensity (km/mole)</p> <p>Frequency (1/cm)</p>
CoFe <sub>2</sub> B <sub>3</sub>	 <p>IR Intensity (km/mole)</p> <p>Frequency (1/cm)</p>
Fe <sub>2</sub> Co <sub>2</sub> B <sub>2</sub>	 <p>IR Intensity (km/mole)</p> <p>Frequency (1/cm)</p>
Fe <sub>2</sub> Co <sub>3</sub> B	 <p>IR Intensity (km/mole)</p> <p>Frequency (1/cm)</p>

Table 6.2.3. Spectrum for large clusters  $\text{Fe}_x\text{Co}_y\text{B}_z$  in model 3 of chapter 6.

Cluster	Spectrum
$\text{FeCo}_2\text{B}_4$	
$\text{FeCo}_4\text{B}_2$	
$\text{Fe}_2\text{CoB}_4$	
$\text{Fe}_2\text{Co}_4\text{B}$	

Table 6.2.3. Continued

Cluster	Spectrum
$\text{Fe}_4\text{Co}_2\text{B}$	
$\text{Fe}_4\text{CoB}_2$	
$\text{FeCo}_3\text{B}_3$	
$\text{Fe}_3\text{CoB}_3$	

Table 6.2.3. Continued

Cluster	Spectrum
$\text{Fe}_3\text{Co}_3\text{B}$	<p>IR Intensity (km/mole)</p> <p>Frequency (1/cm)</p>
$\text{Fe}_2\text{Co}_2\text{B}_3$	<p>IR Intensity (km/mole)</p> <p>Frequency (1/cm)</p>
$\text{Fe}_3\text{Co}_2\text{B}_2$	<p>IR Intensity (km/mole)</p> <p>Frequency (1/cm)</p>

Table 6.2.4. Spectrum for large clusters  $\text{Fe}_x\text{Co}_y\text{B}_z$  in model 4 of chapter 6.

Cluster	Spectrum
$\text{FeCo}_3\text{B}_4$	
$\text{Fe}_3\text{CoB}_4$	
$\text{Fe}_3\text{Co}_3\text{B}_2$	
$\text{Fe}_3\text{Co}_4\text{B}$	
$\text{Fe}_4\text{Co}_3\text{B}$	

Table 6.2.5. Spectrum for large clusters  $\text{Fe}_x\text{Co}_y\text{B}_z$  in model 5 of chapter 6.

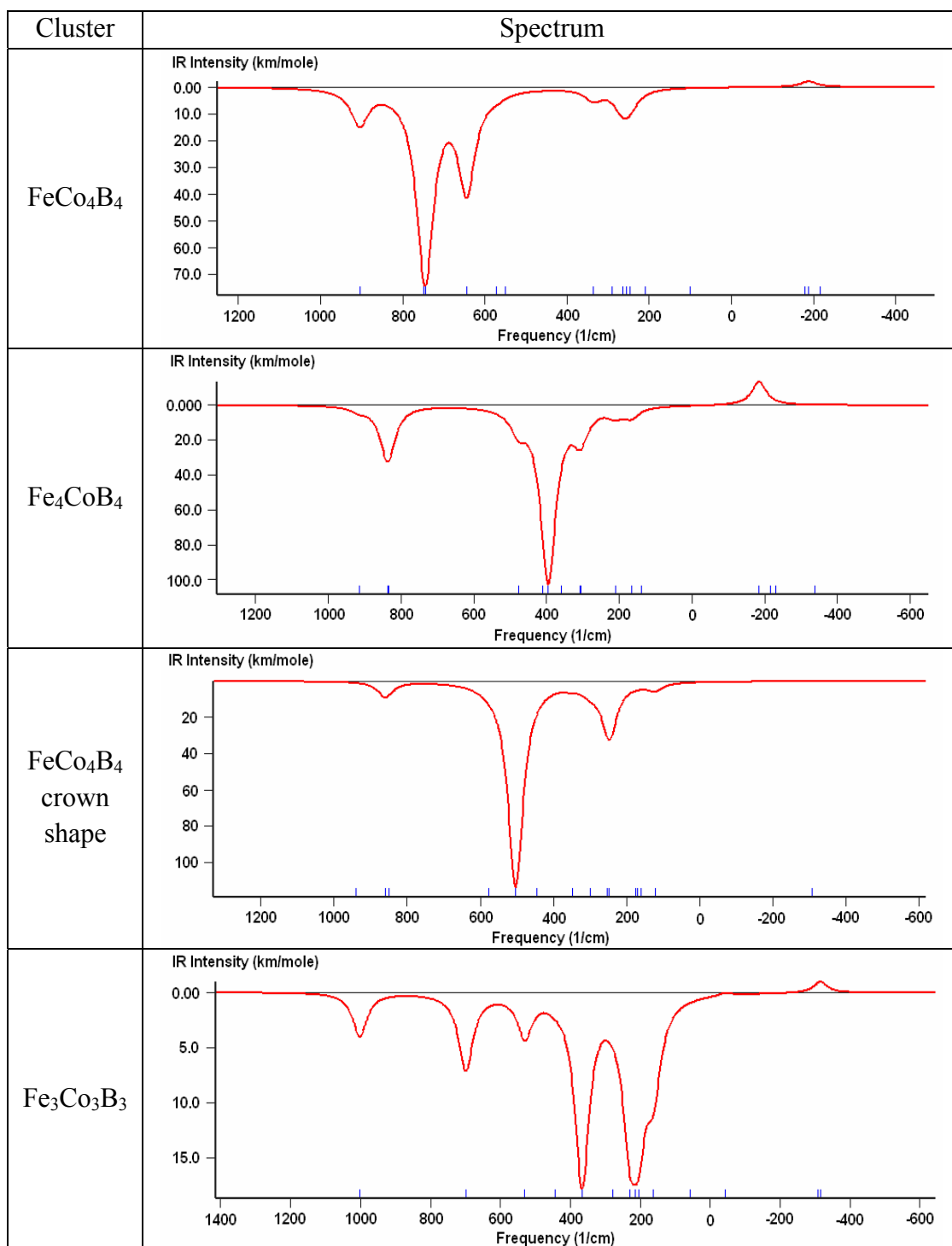


Table 6.2.6. Spectrum for large clusters  $\text{Fe}_x\text{Co}_y\text{B}_z$  in model 6 of chapter 6.

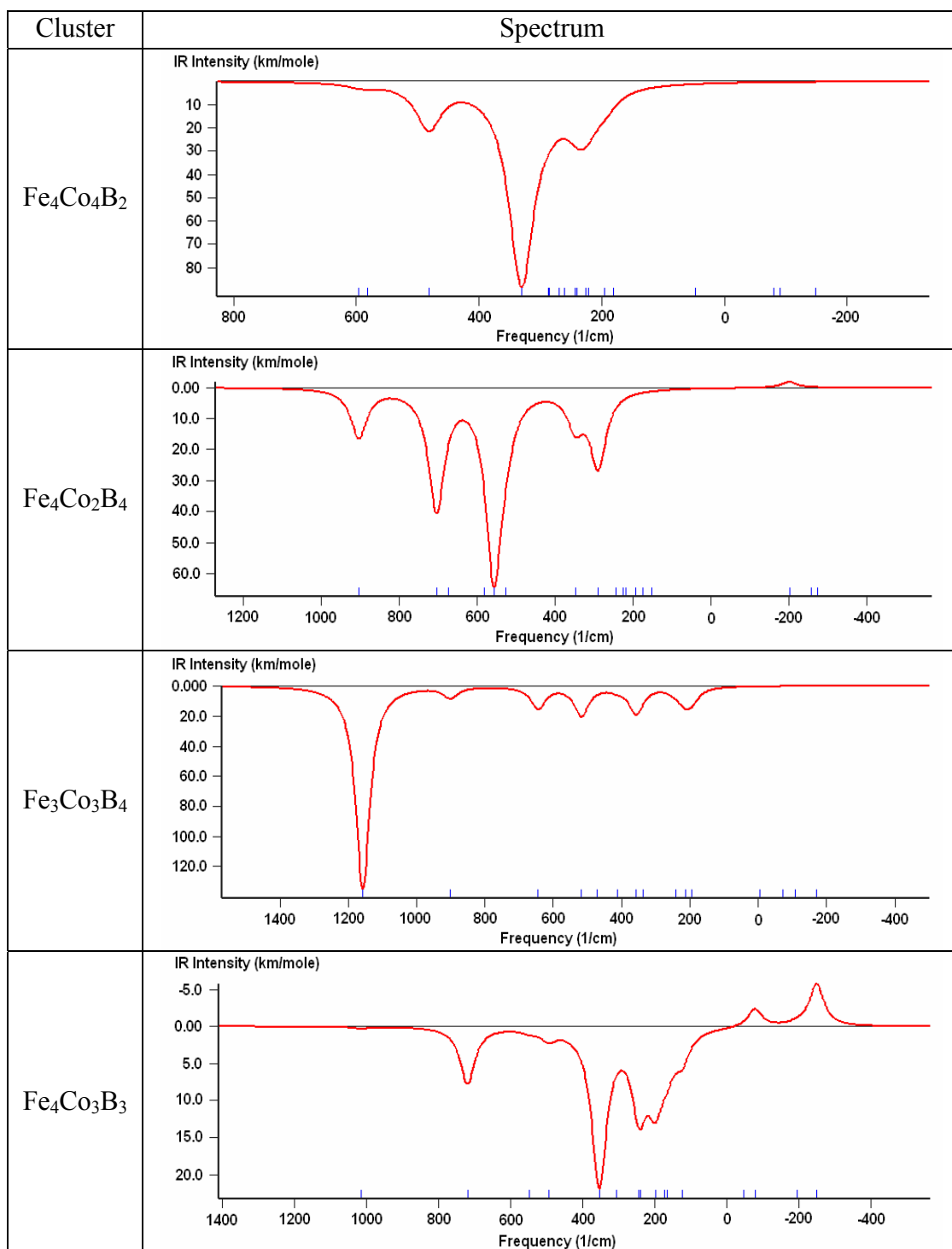
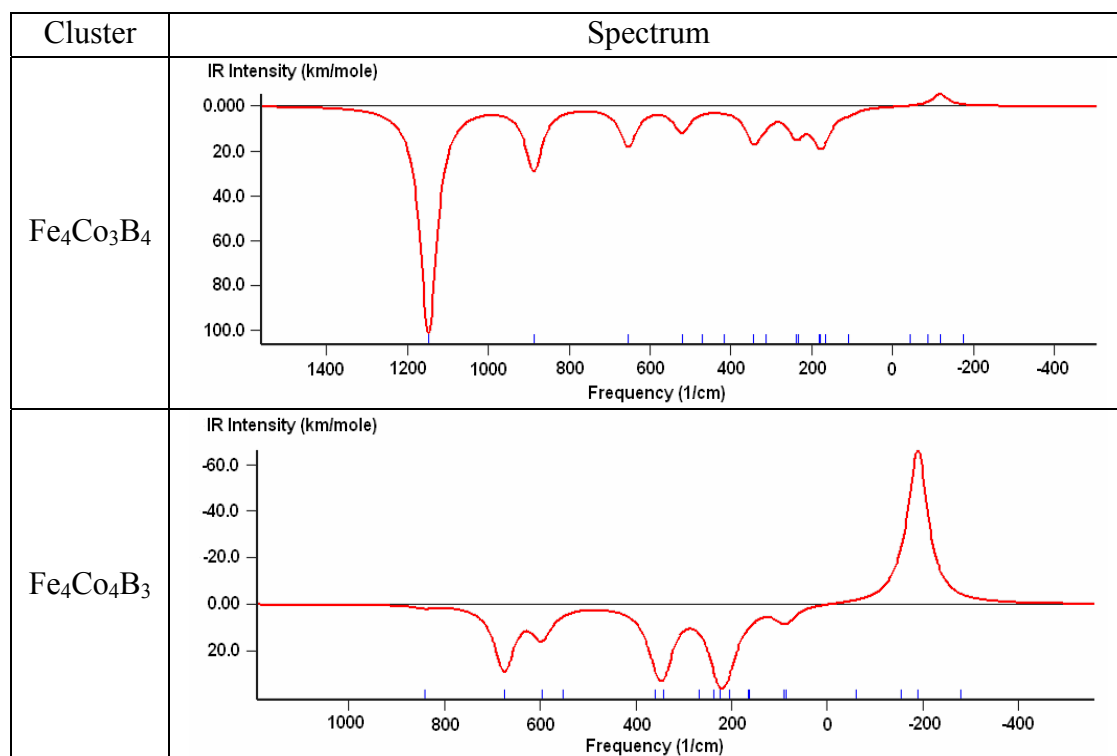


Table 6.2.7. Spectrum for large clusters  $\text{Fe}_x\text{Co}_y\text{B}_z$  in model 7 of chapter 6.





# Bibliography

- [1] J. Raffel and T. Crowder (1964). *IEEE Trans. Electronic Components* 13, No. 5, p. 611
- [2] M. Johnson, B. Bennett and M. Yang (1998). Hybrid Ferromagnetic Semiconductor Nonvolatile Memory, *IEEE Trans. Magn.* 34, no.4, pp 1054-1059.
- [3] Johan Akerman (2005). Toward a Universal Memory. *Science*, **308**, no. 5721, pp. 508-510.
- [4] K. Itoh (2001). VLSI Memory Chip Design. *Springer-Verlag*.
- [5] M. N. Baibich *et al.* (1988). Giant Magnetoresistance of (001)Fe/(001)Cr Magnetic Superlattices. *Phys. Rev. Lett.*, **61**, 2472.
- [6] H. Kaakani (Mar. 10-17, 2001). Radiation Hardened Memory Development at Honeywell. *IEEE Aerospace Conference*, Big Sky MT, **5**, 2273-2279.
- [7] G. Prinz (1998). Magnetoelectronics. *Science*, **282**, no. 5394, pp. 1660-1663.
- [8] B. Prince (2002). Emerging Memories-Technologies and Trends. Kluwer, Norwell, MA.
- [9] S. Tehrani *et al.* (8-11 Dec 1996). High Density Nonvolatile Magnetoresistive RAM. *IEDM*, San Francisco, pp. 193-196.
- [10] J. DeBrosse *et al.* (Apr. 2004). A High-Speed 128-kb MRAM Core for Future Universal Memory Applications. *IEEE JSSC*, **39**, no. 4, pp. 678-683.
- [11] S. Tehrani *et al.* (Sept. 1999). Progress and Outlook for MRAM Technology. *IEEE Trans. Magnetism*, **35**, no. 5, pp. 2814-2819.
- [12] S. Tehrani *et al.* (Sept. 2000). Recent Development in Magnetic Tunnel Junction MRAM. *IEEE Trans. Magnetism*, **36**, no. 5, pp. 2752-2757.
- [13] S. Tehrani *et al.* (May 2003). Magnetoresistive Random Access Memory Using Magnetic Tunnel Junctions. *Proc. IEEE*, **91**, no. 5, pp. 703-714.
- [14] L. H. Thomas (1927). The calculation of atomic fields. *Proc. Camb. Phil. Soc.*, **23**, 542-548.
- [15] E. Fermi (1927). Un Metodo Statistico per la Determinazione di alcune Priorieta dell'Atome. *Rend. Accad. Naz. Lincei*, **6**, 602-607.

- [16] E. Fermi (1928). A statistical method for the determination of some atomic properties and the application of this method to the theory of the periodic system of elements. *Z. Phys.*, **48**, 73-79.
- [17] E. Fermi (1928). Sulla deduzione statistica di alcune proprietà dell'atomo. Applicazione alla teoria del sistema periodico degli elementi. *Rend. Accad. Naz. Lincei*, **7**, 342-346.
- [18] I. Schiff (1986). *Quantum Mechanics*. McGraw-Hill.
- [19] W. Kohn and L. J. Sham (1965). *Phys. Rev.*, **140**, A1133.
- [20] Orthmann, F., Schmidt, W. G. and Bechstedt, F. (2005). Attracted by long-range electron correlation: adenine on graphite. *Phys. Rev. Lett.*, **95**, 186101.
- [21] Shrivastava, K. N. *et al.* (1999). Density functional theory calculations of molecular nitrogen on a ruthenium cluster. *Chem. Phys. Lett.*, **313**, 279.
- [22] Shrivastava, K. N. *et al.* (2000). Density functional theory of potassium atoms in zeolite. *Chem. Phys. Lett.*, **325**, 1.
- [23] Jeanne L. McHale (1999). *Molecular Spectroscopy*. Prentice Hall.
- [24] N. B. Colthup, L. H. Daly, S. E. Wiberley (1990). Introduction to infrared and Raman Spectroscopy 3<sup>rd</sup> edition. *Academic Press, Boston*.
- [25] P. Gans (1971). *Vibrating molecules*. Chapman and Hall.
- [26] S. van Dijken, X. Jiang and S. P. S. Parkin (2002). *Phys. Rev. B.*, **66**, 094417.
- [27] Y.-T. Cui, J. C. Sankey, C. Wang, K. V. Thadani, Z.-P. Li, R. A. Buhrman and D. C. Ralph (2008). *Phys. Rev. B.*, **77**, 214440.
- [28] B. S. Kessler and A. S. Arrott (2005). *J. Appl. Phys.*, **97**, 10C502.
- [29] S. C. Oh, J. E. Lee, H.-J. Kim, Y. K. Ha, J. S. Bae, K. T. Nam, E. S. Kim, S. O. Park, H. S. Kim, V-In Chung and J. T. Moon (2005). *J. Appl. Phys.*, **97**, 10P509.
- [30] D. Lopez-Duran, M. P. de Lara-Castells, G. Delgado-Barrio, P. Villarreal, C. Di. Paola, F. A. Gianturco and J. Jellinek (2004). *Phys. Rev. Lett.*, **93**, 053401.
- [31] W. Kohn and L. J. Sham (1965). *Phys. Rev.*, **137**, A1697.
- [32] L. J. Sham and W. Kohn (1965). *Phys. Rev.*, **145**, 561.
- [33] W. Kohn (1999). *Rev. Mod. Phys.*, **71**, 1253.
- [34] H. A. Kassim, I. A. Jalil, N. Yusof, V. R. Devi and K. N. Shrivastava (2007). *J. Non-Cryst. Solids*, **353**, 111-118.

- [35] N. A. Jemali, H. A. Kassim, V. R. Devi and K. N. Shrivastava (2008). *J. Non-Cryst. Solids*, **354**, 1744-1750.
- [36] A. N. Rosli, H. A. Kassim and K. N. Shrivastava (2008). *AIP Conf. Proc.*, **1017**, 429-433.
- [37] W. Rudzinski (2007). *Rev. Adv. Mater. Sci.*, **14**, 66-70